On the bramble way to Mg metal anodes in secondary Mg ion batteries.

ZOU, G., FENG, J., ZHAO, X., WANG, J., WANG, Y., YANG, W., WEI, M., WANG, Y., LI, L., REN, L., FERNANDEZ, C. and PENG, Q.

2023

Review Article

On the bramble way to Mg metal anodes in secondary Mg ion batteries

Guodong Zou [a, 1, *], Jiawen Feng [a, 1], Xue Zhao [a], Jinming Wang [a], Yangyang Wang [a], Weihao Yang [a], Mengyao Wei [a], Yimin Wang [b], Lanjie Li [c], Liqun Ren [d], Carlos Fernandez [e], Qiuming Peng [a, *]

[a]   State Key Laboratory of Metastable Materials Science and Technology, School of Materials Science and Engineering, Yanshan University, Qinhuangdao 066004, China

[b]   Department of General Surgery, First Hospital of Qinhuangdao, Hebei Medical University, Qinhuangdao 066000, China

[c]   Chengde Iron and Steel Group Co., Ltd., HBIS Group Co., Ltd., Chengde 067102, China

[d]   Laboratory of Spinal Cord Injury and Rehabilitation, Chengde Medical University, Chengde 067000, China

[e]   School of Pharmacy and Life Sciences, Robert Gordon University, Aberdeen, AB107GJ, United Kingdom

*Corresponding authors.

E-mail addresses: zouguodong@ysu.edu.cn (G.D. Zou), pengqiuming@ysu.edu.cn (Q.M. Peng).

[1]These authors contributed equally to this work.

Abstract

As a prospective alternative to lithium-ion batteries, rechargeable magnesium metal batteries (RMBs) have many unparalleled advantages, including direct use of Mg metal as the electrode; large nature abundance; intrinsically safe merits; high theoretical volumetric capacity. Nonetheless, there exist a large number of challenges on electrodes for their applications. Among them, surface passivation, uneven deposition/dissolution, and corrosion are critical issues that severely hinder the development of Mg anodes in RMBs. This review gives a specific, comprehensive, and in-depth summary of mechanisms relative to these problems. Subsequently, it displays the protection progresses of the Mg metal anode via three-dimensional host nanostructure fabrication, Mg alloys anode design, current collector modification, artificial solid-electrolyte interphase construction, and electrolyte optimization. Finally, future perspectives and outlooks in developing the other blossom of these strategies for rechargeable Mg batteries are also discussed. This overview provides significant guidance for designing and fabricating high-performance Mg metal anodes in secondary Mg batteries and boosting their commercial applications.

1. Introduction

Owing to the scarcity and non-reproducibility of fossil fuels, the requirement for renewable energy is a pressing concern [1, 2]. The importance of low-cost, safe, and easily manufactured electrochemical energy storage and conversion systems has emerged, with lithium-ion batteries (LIBs) being the most successful commercially [3]. However, the use of lithium metal electrodes is limited by their thermodynamic stability in electrolytes. In fact, most metals work irreversibly in conventional electrolytes because of the formation of passivation layers on the metal surface that hinder ionic or electronic conduction. Furthermore, the interplay among uniform ion transport, the roughness of the metal electrodes, and the wettability of the separator can create an inhomogeneous electric field between the electrodes in electrolytes with low cation transfer coefficients, leading to continuous electrolysis or deposition [4]. In order to successfully realize metal electrode-based batteries, metal anodes with high reversibility during deposition and dissolution are needed.

Rechargeable magnesium-metal batteries (RMBs) are based on a new battery technology with magnesium (Mg) metal anodes with unlimited resources and suitable electronegativity and serve as a promising alternative to LIBs [5–8]. Mg metal possesses a high abundance, a volume capacity of 3833 mAh cm^{-3} and gravimetric capacity of 2205 mA h g^{-1}, and low redox potential (-2.37 V vs. SHE) [9]. Using Mg as an anode of the battery has the advantages of low cost and large capacity. Although the concept of RMBs consisting of Mg metal anode and Co_3O_4 cathode was proposed by Gregory et al. [10] in 1990, RMBs still have many common problems with Mg

metal electrodes [11, 12]. Many groups have demonstrated Mg uneven deposition or detrimental Mg dendrites instead of the "non-dendrite" forming nature of the Mg metal anode. Therefore, the nonuniformly electrodepositing of Mg metal anode should be overcome in the practical RMBs in case of safety problems. The thermodynamic origin of dendrite growth in Mg metal anode batteries is a complex phenomenon. It is confirmed that the thermodynamic origin of the epitaxial, mossy, and fractal Mg dendrite growth regimes are connected with the intrinsic energetic properties of Mg metal surfaces [13, 14]. Accordingly, high surface tension, low surface capacitance, and low potential of zero-charge are in favor of dendrite-free Mg anodes and can be obtained through appropriate chemical engineering. When the Mg electrode is in contact with most conventional anions in an electrolyte (such as ClO_4^-, PF_6^-, and BF_4^-) or reducing substances such as oxygen and water, the surface passivation film is easily formed on the surface of Mg [15]. The passivation film cannot conduct Mg^{2+} ions, inhibiting redox reactions at the Mg anode and slowing the kinetics of Mg electrodeposition. Furthermore, due to concerns with the reductive ability of water on Mg, a huge research gap exists in tackling the passivation chemistry of Mg in aqueous electrolytes, such that Mg can be directly employed as anodes to reduce the costs and boost the kinetics of RMBs [16–18]. Therefore, in-depth study and optimization of Mg anodes are necessary for RMBs to move toward commercial applications.

In recent years, to further improve the electrochemical performance of Mg metal anode, various strategies have been developed, including three-dimensional (3D) host

nanostructure design, Mg alloys anode engineering, surface modification, and electrolyte optimization [19]. Fig. 1 depicts a timeline of the development of modification strategies for Mg metal anodes [7, 11, 16, 20–28]. For structural design, many efforts have been made to build a 3D Mg anode, which may considerably reduce the formation of Mg dendrites by increasing active specific surface area [29, 30]. With regard to Mg alloys' anode engineering, various elements and microstructures of Mg alloys play a vital role in affecting the performance of RMBs. In the case of surface modification, it generally takes the form of several types of protective layers which utilize various mechanisms. Similarly, for electrolytes, Mg^{2+} stripping/plating behaviors on the Mg anode surface are primarily controlled and modified by electrolyte regulation [27, 30–32]. To our knowledge, the recent advances in regard to the strategies for the stabilization of Mg metal anodes were rarely reported [33, 34].

Herein, we comprehensively summarize the latest development of Mg anode modifications strategies for RMBs (as shown in Fig. 2). Firstly, the main challenges, including surface passivation, uneven deposition/dissolution, and corrosion, are systematically analyzed to identify Mg deposition behavior at Mg metal anode. In addition, various recent modifications strategies to enhance the Mg metal anode performance are categorized and discussed in detail, involving Mg metal anode engineering (3D host nanostructure fabrication, Mg alloys anode design, and current collector modification), artificial solid-electrolyte interphase (SEI) construction, and electrolyte optimization (organic electrolyte, solid-state electrolyte, and aqueous

electrolyte). Finally, by analyzing the latest research achievements, future perspectives on Mg metal anode are also presented. Hopefully, this review could inspire researchers to explore more modification strategies of Mg metal anodes for RMBs and promote their commercial applications.

2. Current challenges for Mg metal anode

The electrochemical property of RMBs is highly dependent on the possible interface reactions between the Mg metal anode and electrolytes. In general, the RMBs involve the reversible Mg^{2+} ions deposition/dissolution on the surface of the Mg metal anode on the condition of the charging/discharging procedure [35]. Mg metal anode with high electrochemical activity and thermodynamical instability in common electrolytes can suffer from heavy parasitic reactions, resulting in various issues on Mg metal anode [36]: surface passivation, uneven Mg deposition/ dissolution, and corrosion which will be analyzed as follows.

2.1. Surface passivation

The surface passivation of the Mg metal anode is a significant concern for RMBs. Mg surface passivation comes from two aspects. On the one hand, strong coordination with cations gives rise to the solvents/anions becoming easy to decompose in the vicinity of the Mg metal anode. Then, a thick passive film would be generated on the Mg metal anode [2, 37, 38]. On the other hand, Mg metal is susceptible to reacting with air and water. Therefore, the surface of as-received Mg metals consists of substantial passivation layers, which are hard to remove. These poor surface passivation films composed of Mg^{2+}-insulating inorganic, such as MgO, $Mg(OH)_2$, or

MgCO$_3$, *etc*., will lead to sluggish Mg^{2+} transport, low Coulombic efficiency, and a large voltage hysteresis in RMBs [39].

2.2. Uneven Mg deposition/dissolution

Uneven Mg deposition during charging is of great significance for affecting the degradation of the Mg metal anode. Generally, uneven Mg deposition with hemispherical and porous morphology could trigger severe parasitic reactions, causing performance decay and safety concerns. Recently, uneven Mg deposition with dendritic morphologies was reported, which may be originated from certain electrolytes utilization (such as Grignard reagents, Mg(TFSI)$_2$-based electrolyte, *etc*.) or the high applied current density and large areal capacity [24, 27, 40, 41]. The formation of Mg dendrites increases the risk of penetrating the separator, resulting in internal short-circuiting, battery failure, and safety issues. In this regard, Mg deposits with smooth and compact morphology are preferable to the uneven Mg deposition for Mg metal anode. Moreover, the 'dead' Mg forms when Mg dendrites peel off during the stripping process, which displays low Coulombic efficiency, large voltage hysteresis, and poor battery rechargeability, leading to the failure of the Mg metal anode. In addition, uneven Mg stripping under moderate current density is observed by Cui's group [28], which severely destroys the anode integrity and Mg deposition homogeneity, causing the degradation of the Mg metal anode. Therefore, we must consider the Mg metal anode's deposition/stripping process for practical application.

2.3. Corrosion

Corrosion of Mg metal anodes is another critical factor influencing the

performance of RMBs, which can be mainly classified as self-corrosion and electrochemical corrosion. In an aqueous electrolyte, the Mg metal anode is apt to dissolute over a pH range from 0 to 10.5 [42–44]. Due to a more negative potential (–2.37 V *vs*. SHE) for Mg metal anodes than hydrogen, the self-corrosion in aqueous electrolyte happens by itself, which logically can correspond to the hydrogen evolution phenomenon, leading to suffering poor anodic efficiency and low discharge voltage in Mg-metal batteries [16, 17, 24, 45]. In terms of electrochemical corrosion, the formation of the irreversible consumption and inert by-products accumulated on the surface of the Mg anode after repeated cycling can be observed, resulting in poor electrochemical performance due to anode polarization and mechanical integrity.

3. Mg metal anode engineering

3.1. Three-dimensional (3D) host nanostructure fabrication

Recent studies have found that the 3D host can effectively suppress the uneven Mg deposition/dissolution or dendrite growth by dramatically decreasing the local electric field and blocking the vertical growth toward the cathode. Moreover, it mitigates the change in volume of the Mg metal due to its porous structure and high surface area [8, 46, 47]. For example, magnesiophilic 3D MgBi scaffolds were employed for reversible Mg plating/stripping, which facilitated the passivation layer to convert into a stable SEI film [48]. Compared with Mg foils, the high surface area of 3D Mg_3Bi_2 scaffolds reduced the effective current density to avoid continuous electrolyte decomposition (Fig. 3(a)). Meanwhile, Mg_3Bi_2 displayed a small nucleation energy barrier owing to the bonding reaction with pure Mg, which can

8

guide the uniform deposition of Mg on the scaffold (Fig. 3(b, c)).

The effects of the electric field effect, chemisorption effect, and substrate geometry on the electrodeposition morphology of Mg anodes were investigated. Song *et al*. [49] proposed a carbon cloth composed of a vertically aligned nitrogen and oxygen-doped carbon nanofiber array-constructed 3D host (denoted as VNCA@C) for uniform Mg electrodeposition. The chemisorption ability of the carbon-based substrate toward metal atoms or metal ions has a significant effect on controlling the preferential nucleation sites for metal growth, which can be regulated by changing surface functional groups on the carbon-based substrate. The doping atom with a more negative charge state should form an electronegative site to induce a stronger interaction with the Mg^{2+} ions [50]. The VNCA@C substrate with abundant magnesiophilic sites (nitrogen and oxygen) enhanced the Mg atoms affinity, which tremendously decreased the nucleation and growth energy barriers resulting in lower Mg stripping/plating overpotentials (Fig. 3(d)). At a high current density of 10.0 mA cm^{-2}, the nucleation overpotential is reduced by 647 mV, and the Mg plating/stripping cycle life is extended by 110 cycles using the VNCA@C host (Fig. 3(e)). The synergistic coupling of uniform current distribution, geometric confinement, and chemisorption effect in the nitrogen/oxygen doping 3D host could effectively prevent the uneven Mg electrodeposition.

The dilemma between anodic Mg^{2+} plating/stripping and cathodic oxidation stability hinders RMBs from achieving high energy density in practical applications. To overcome these limitations, an amorphous MgO-wrapped Zn 3D framework was

designed as a unique current collector for anode-free RMBs to achieve Mg^{2+} plating/stripping [51]. Owing to the fast kinetics and excellent stability of the anode interface, the constructed Mg-Li hybrid battery with antioxidant electrolyte exhibited excellent electrochemical performance with an operating voltage of 2.82 V *vs.* Mg/Mg^{2+} and a promising energy density of 412.5 Wh kg^{-1} (Fig. 3(f)). In addition, the epitaxial electro-crystallization of Mg onto a 3D magnesiophilic host through the synergy of magnesiophilic interface, lattice matching, and electrostatic confinement effects was conceived [52]. Vertically aligned nickel hydroxide nanosheet arrays (referred to as $Ni(OH)_2$@CC) grown on carbon cloth were designed as efficient 3D magnesiophilic hosts for RMBs. Under practical conditions (10 mA cm^{-2} and 10 mA h cm^{-2}), $Ni(OH)_2$@CC substrates exhibited stable Mg stripping/plating cycling performance over 600 h, which was better than pristine copper foil and carbon cloth substrates two orders of magnitude higher.

It was demonstrated that Ag nanoparticles (AgNPs) had strong affinity as Mg deposits through *in-situ* and *ex-situ* observations [53]. As the magnesiophilic sites of AgNPs were favorable for uniformly attaching the newly deposited Mg on the surface of designed Ag-decorated copper foams (ACFs), ACFs exhibited excellent electrochemical performance, including low nucleation overpotential, high cyclability, and improved rate capability compared with bare CF.

3.2. Mg alloys anode design

Up to now, the mechanical and physical properties of Mg metal have been intensively studied in structural materials [12, 54]. Microstructural factors of Mg

metals and alloys mainly determine their physical and mechanical properties; thus, electrochemical properties can also be altered by metallurgical manipulations, which have been considered one of the most promising strategies for Mg metal anodes protection in RMBs (Table 1). The effect of metallurgical characteristics on the electrochemical performances of Mg metal anodes was investigated [55–57]. The crystal orientation had an essential effect on the activity, and the (0001) plane crystals exhibited favorable properties because the (0001) direction showed a larger specific conductivity than the (10$\bar{1}$0) direction (Fig. 4(a)). The electrochemical performance of Mg anodes can be improved by suitable control of the crystallographic orientation related to alloying (Fig. 4(b)). The electrochemical process of Mg^{2+}/Mg^{0} had a strong correlation with the grain boundary properties [55].

The low ductility of pure Mg metal makes it challenging to fabricate very thin Mg foil electrodes [58, 59]. Alloying helps to tune the mechanical and structural properties of Mg anodes, as well as improves their processability. The feasibility of replacing pure Mg foils with AZ31 alloy foils (3% Al and 1% Zn) as the anode was investigated [39]. It was found the electrochemical and surface chemical behavior of AZ31 thin foil anodes during the Mg dissolution/deposition process was extremely similar to pure Mg foils anodes, and the morphology after the Mg dissolution or deposition process was more uniform. In addition, excellent compatibility of ultrathin AZ31 Mg alloy anodes (~25 μm thick) and the $Mg_xMo_6S_8$ phase cathode was demonstrated in full-cell tests. Using ultrathin processable Mg alloy anodes is an important step toward high-energy-density RMBs. To improve the processability of

Mg alloys, the alloying Zn and Gd elements were introduced in Mg metal and made as anodes for RMBs [23]. Mg-1.63 wt% Zn, Mg-1.55 wt% Gd, and Mg-1.02 wt% Zn-1.01 wt% Gd were investigated for the electrochemical behavior. The alloying elements were not only dissolved in the electrolyte but also easily redeposited. At the cathodic potential, not only Mg precipitated out of the electrolyte, but also Zn and Gd dissolved during the anodic half-cycle. While the co-deposition of alloying elements plays a vital role in aqueous Mg corrosion and hydrogen evolution, its effect on the anode performance of non-aqueous secondary Mg batteries appears negligible [23].

The actual energy density of RMBs is still limited by the passivation of the Mg anode. Alloying strategies are tailored to avoid the passivation of the Mg anode. Recently, using Mg-Li alloys as anodes, Li with high reactivity reacted with Mg^{2+} ions in the $Mg(TFSI)_2$/DME electrolyte, thus hindering the formation of a passive film on the anode surface [60]. The results illustrated that most Mg and a small amount of Li were stripped off during the electrochemical oxidation of the Mg-Li alloy anode, which proved that the substitution reaction at the Mg-Li alloy anode/electrolyte interface hindered the formation of the passivation film (Fig. 4(c)).

The development of high-performance Mg alloy anodes that can operate in conventional electrolytes could be a key breakthrough in the viability of RMBs. Based on the alloying reaction between Mg and Sn, the Mg anode was replaced by Sn and Mg_2Sn, and the electrochemical performance of four hypoeutectic Mg-Sn alloy anodes was investigated [61]. Mg^{2+} ions were reversibly deposited/dissolute on the surface of Mg and Mg-Sn alloy electrodes. With the increase of Sn content, the

12

eutectic (α-Mg + Mg_2Sn) phase was formed in the grain boundary and dendrite region of the Mg-14Sn alloy. The significant reduction in anode-electrolyte interfacial resistance after Sn addition was mainly owing to the formation of β-Sn particles during the dealloying process of Mg_2Sn in the eutectic phase. In similar work, MgSn alloys can be used as a high-performance anode for RMBs [57]. The resulting MgSn alloys consisted of crystalline Mg-rich (c-Mg), amorphous Mg-rich (a-Mg), and intermetallic Mg_2Sn phases. Large amounts of Mg^{2+} ions were produced even at high rates in non-Grignard and Lewis acid-free electrolytes. Besides the favorable effect of c-Mg on the electrochemical performance of Mg/Mg_2Sn in the half-cell structure, the irreversibly dissolved Mg^{2+} ions can ideally balance the trapped Mg^{2+} ions in the Mo_6S_8 cathode in the full cell.

3.3. Current collector modification

RMBs can use not only free Mg metal foils as the anode but also use an Mg-deposited porous current collector (*e.g.*, Cu) as the anode to assemble the full battery. For pre-deposited Mg metal batteries, the current collector serves as the connection between the active material of the anode and the external circuit, and acts as the substrate for Mg plating, besides, plays a vital role in the Mg nucleation and growth and accordingly the battery performance. Nevertheless, the commonly used planar Cu current collector does not work satisfactorily, therefore, some modifications of the Cu current collector have been reported in the literatures to reduce the local current density, prevent the Mg dendrite growth, and improve the Coulombic efficiency.

Recently, a new strategy to regulate dendritic growth was proposed by introducing the magnesiophilic gold (Au) nano-seeds on the Cu foils [27]. Density functional theory (DFT) calculations were also carried out to understand the role of the magnesiophilicity of the Au atom. It was proved that Au nano-seeds can effectively inhibit dendrite growth because of the relatively low diffusion barrier of the Mg atom. Besides, the dynamic growth of Mg dendrites was proved by various *operando* observation techniques, and the critical current density that can trigger short circuits was defined at a relatively low rate of 2 mA cm^{-2}, and the substrate was covered by a large number of spherical Mg seeds. In contrast, fatal needle-like dendritic growth was clearly observed at a critical current density of 10 mA cm^{-2} (Fig. 5). The changed growth mechanism not only helped to suppress the Mg dendrites growth but also decreased the nucleation polarization and finally slowed down the occurrence of short circuit. Besides, a modified commercial Cu foil with magnesiophilic Au nanocoating was designed to realize deeply cycled composited Mg anodes with an unprecedented 75% Mg anode utilization [29]. The Mg-coated Au-Cu electrode exhibited a high average Coulombic efficiency of 99.16% over 170 h cycling with 75% Mg anode utilization compared to its bare Cu counterpart. These works shed light on the rational design of composite Mg anodes with high utilization and reversibility, driving the development of high-energy-density RMBs in the future.

A 3D Cu grid with nanowires and magnesiophilic Ag sites (denoted as Ag@3D Cu grids) was developed as a high-performance and low-cost current collector to tune Mg deposition behavior and achieve uniform Mg electrodeposition [62]. The Ag@3D

Cu grid collector displayed significantly reduced nucleation overpotentials at current densities of 1.0 and 8.0 mA cm^{-2} and operated stably even at a high current density of 8.0 mA cm^{-2}. *In situ* optical images revealed that the reason for the rapid short-circuit of common current collectors at 8.0 mA cm^{-2} was the random growth of large Mg protrusions, but a smooth surface can be obtained with Ag@3D Cu grids.

To date, the current collector engineering research is still in its infancy, and its electrochemical performance in RMBs is far from practical application, especially in the case of high Mg metal utilization [63–66].

4. Artificial solid-electrolyte interphase

RMBs require electrolytes that are thermodynamically stable at low potentials, which is often achieved with corrosive components and at the expense of oxidative stability [67–69]. However, the conflict between the cathodic and anodic stability of the electrolyte cannot be resolved in Mg batteries by forming an anodic interface that protects the electrolyte from reduction because divalent Mg^{2+} cannot penetrate such an interface [70]. It is found that high surface coverage and ionic conductivity can be achieved by tuning the properties of the interface material on the reactive metal surface to protect Mg anodes from reactive electrolyte solutions [71, 72]. The Mg^{2+} ion-conducting artificial interface enables highly reversible Mg deposition and exfoliation in conventional electrolytes. To date, the reported Mg-ion conductive SEI film mainly includes three categories: organic, inorganic, and hybrid artificial solid-electrolyte interphase (ASEI).

4.1. Organic artificial SEI

RMBs are one of the most promising candidates for next-generation batteries due to their safety, low cost, and high energy density. However, the passivation of Mg anodes by forming ion-blocking interfacial layers in conventional organic electrolytes requires Mg-compatible electrolytes [73–75]. Therefore, an easy-to-process method to fabricate a Mg^{2+} ions permeation protective polymer layer to protect Mg metal anodes was proposed [32, 76]. Anionic grafting of bis-trifluoromethanesulfonimide (TFSI) onto a poly(vinylidene fluoride-co-hexafluoropropylene) (PVDF-HFP) polymer backbone resulted in an amorphous structure, which could cover the surface of Mg metal to isolate the electrolyte and improve the conductivity of Mg^{2+} ions through the polymer layer. The Mg anode with the Mg^{2+} ions permeation protective layer exhibited a significant improvement in the performance of Mg symmetric cells and Mg/V_2O_5 full cells. Moreover, the TFSI anion-grafted PVDF-HFP interface can also protect Mg from water.

The composition of the electrolyte is highly resistant to reduction but easily oxidized and highly corrosive, hindering the possibility of Mg batteries operating above 3.0 V. An artificial Mg^{2+} conducting interface made of thermal-cyclized polyacrylonitrile (cPAN) and Mg trifluoromethanesulfonate ($Mg(CF_3SO_3)_2$) was designed on the Mg anode surface which facilitated the reversible Mg deposition/stripping process (Fig. 6(a)). The electronically insulating polymer interface of the Mg metal surface can effectively prevent the electrochemical reduction of the electrolyte and the water, while still allows Mg^{2+} migration (ionic conductivity 1.19×10^{-6} S cm^{-1}), thus allowing the use of carbonate solvents which

are more resistant to oxidation [7].

In addition, the electrochemical pretreatment of lithium metal bis(trifluoromethanesulfonimide) lithium (LiTFSI) in 1,2-dimethoxyethane (DME) and 1,3-dioxofluorenane (DOL) was investigated, and a poly-DOL-based elastomer was formed on the Mg anode as the protective layer of the Mg anode (Fig. 6(b)) [77]. The pretreated Mg anodes exhibited low and stable overpotentials (0.5 V) at current densities (charge capacities) of 0.03 mA cm^{-2} (0.50 mA cm^{-2}) in the Mg(TFSI)$_2$-based conventional electrolytes which suffered from severe dendrite growth [41]. They cycled for 400 h, demonstrating far better electrochemical performance than pristine Mg cycle performance (Fig. 6(c, d)). The enhanced cycling performance was attributed to the soft-rigid nature of ASEI, which was able to suppress the growth of Mg dendrites while conducting Mg^{2+} ions during cycling.

Preventing solvent penetration to the anode surface will fundamentally reduce the strong electrostatic interaction between Mg^{2+} and solvent, and hinder the formation of passivation film, which requires the formation of a film with high selectivity on the Mg surface to reject the solvent molecules of angstrom-size while allowing the transport of Mg^{2+} [19, 36]. Metal-organic framework (MOF) membranes have controllable pore structures and Angstrom-sized pore windows, so MOF-based ion-selective permeable membranes are well suited for sieving solvents at the ionic/molecular scale. A large-area and defect-free MOF film directly on the surface of a Mg anode was constructed by the electrochemical deposition method [78]. Under the protection of the MOF film, a low stripping overpotential of 0.27 V can be

achieved compared to the bare Mg electrode (1.54 V) in the conventional DME-based electrolyte, indicating that the constructed MOF film contributes to the low overpotential in electrolytes plating/stripping (Fig. 6(e)).

4.2. Inorganic artificial SEI

Research on RMBs has been hindered by the difficulty of electrolyte/solvent selection [79, 80]. At low potential, the solid electrolyte interfacial layer formed in Mg batteries using conventional organic electrolytes can adversely affect performance because the interface prevents Mg^{2+} ion conduction and passivates the surface [35, 81]. Therefore, it is very challenging to find an electrolyte/solvent system with both anodic and cathodic stability for RMBs.

It is known that inorganic fluorides such as magnesium fluoride (MgF_2) are ionic conductors but electronic insulators. The MgF_2 layer not only reduces side reactions with the electrolyte but also allows Mg^{2+} transport in this protective layer, and its high specific surface area facilitates the contact between the electrode and the electrolyte [34]. The voltage stability, Coulombic efficiency, and cycling performance of RMBs are improved by the MgF_2 surface layer

$MgSO_3$ is also introduced as an inorganic artificial interfacial layer on the Mg metal surface using a direct gas chemisorption method [74]. The Mg electrode with the $MgSO_3$ interface exhibited low resistance during electrochemical cycling, thus enabling reversible electrochemical dissolution and deposition reactions even in salt-containing ether-based electrolytes. Theoretical calculations elucidated the working mechanism by which the structural deformation induced by SO_2

18

chemisorption significantly reduced the charge transfer barrier of Mg^{2+} ions. In addition, $MgSiN_2$, MgI_2, $MgBr_2$, $MgSe$, MgS, and $Mg(BH_4)_2$ were predicted as promising inorganic ASEI on account of their suitable electrochemical stability and Mg^{2+} ions mobility [66].

Similar to the construction of ASEI by the solute element alloying for lithium metal anodes, the Mg metal depositing overpotential could also be effectively reduced by alloys ASEI, providing a quasi-equilibrium condition for Mg metal depositing [10, 82]. Previous work has demonstrated that Sn and Mg_2Sn electrodes are compatible with conventional electrolytes for RMBs, enabling higher capacities and lower insertion/extraction voltages. Ion exchange and alloying reactions were employed to form the Sn/Mg_2Sn-based artificial thin films with halide components ($MgCl_2/SnCl_2$) [83]. Modified Mg metal anodes with artificial thin films exhibited rapid Mg^{2+} diffusion, which achieved an ultra-long lifetime of over 4000 cycles (1400 h) at a high current density of 6 mA cm^{-2}, and a low overvoltage of about 0.2 V. In addition, a metal-alloy hybrid Bi-based artificial protective layer was constructed on the Mg metal surface using the ion exchange (Fig. 7(a–d)) [4]. The electrochemical tests and interface characterizations proved that the protected Mg electrode not only effectively suppressed harmful parasitic reactions but also significantly inhibited the inhomogeneous growth behavior during repeated Mg plating/stripping processes (Fig. 7(e–l)). Moreover, both $MgCu_{2-x}S$ and $Mg-O_2$ full cells assembled using modified Mg anodes showed a greatly improved performance due to the protective properties of Bi-based artificial layers.

19

Liquid metals were also proposed to form a suitable ASEI. The stability of Mg metal anodes was improved by simply coating a thin layer of liquid metal Ga on Mg foil [12]. Metal Ga can spontaneously form alloys with metal Mg to form a stable Mg^{2+} conductive, corrosion-resistant, and magnesiophilic Ga_5Mg_2 alloy layer. The Ga_5Mg_2 alloy has low diffusion energy barriers of 1.91 and 2.55 eV for intralayer and interlayer diffusion, indicating that Mg^{2+} has the ability to diffuse rapidly. The alloy exhibited a certain degree of magnesiophilicity due to the presence of magnesiophilic Ga sites in Ga_5Mg_2. The nucleation barrier can be reduced during the Mg plating/striping process, and uniform and dendrite-free Mg deposition can be formed.

4.4. Hybrid artificial SEI

An ideal ASEI for practical RMBs should have the following characteristics: high ionic conductivity and an appropriate thickness to reduce Mg^{2+} ions diffusion resistance, and flexible and good mechanical strength to inhibit the Mg dendrites growth and resist volume change. Hybrid ASEI with both high-ionic-conductivity inorganic and flexible organic have been constructed to protect Mg metal anodes, demonstrating greatly enhanced cycling stability and dendrite suppressing effect [84].

Through the *in situ* chemical reactions of Mg with H_3PO_4 and $SiCl_4$, an artificial interface composed of amorphous (a-)$MgCl_2$@polymer was prepared on the Mg surface, which can effectively suppress electrolyte decomposition and promote Mg^{2+} transport (Fig. 8(a)) [85]. In 0.5 M $Mg(TFSI)_2$/DME electrolytes, Mg||Mg symmetric cells with modified Mg electrodes exhibit lower overpotential (~0.25 V at 0.1 mA cm$^-$^{2}) than bare Mg electrodes and interface impedance (Fig. 8(b–f)). The Mg-Mo_6S_8 full

cell with modified Mg as anode exhibits a higher discharge voltage plateau (~1 V) and lower voltage hysteresis (~0.3 V) at 0.1 C than the bare Mg anode. The Mg-S full battery with modified Mg as the negative electrode can achieve a discharge voltage platform of ~1.5 V, which is greatly improved compared with the bare Mg metal as the negative electrode (~0.5 V), and the specific capacity can be as high as 1000 mA h g^{-1} based on 0.1 C sulfur mass during initial discharge.

5. Electrolyte optimization

To further improve the performance of RMBs, considerable efforts have been devoted to designing new organic electrolytes since the electrolyte is in favor of transferring ions between the cathode and Mg metal anode [86]. To achieve high-performance RMBs, the Mg electrolyte with high ionically conductive for Mg^{2+} ions, reversible deposition and dissolution of Mg, and a wide electrochemical window is indispensable [26]. Another important consideration of electrolytes is safety issues such as good thermal stability, low volatility, low flammability, and environmental friendliness. To date, researchers have developed various electrolytes, including organic electrolytes, solid-state electrolytes, and aqueous electrolytes.

5.1. Organic electrolyte

Unlike in Li-ion batteries, the conventional organic electrolytes in RMBs consist of common commercial Mg salts (such as $Mg(ClO_4)_2$), which are poorly compatible with Mg metal anode due to the formation of a Mg^{2+} nonconductive passivation layer, resulting in not reversible Mg deposition/dissolution [2, 38, 87, 88]. Thus, many significant research efforts have been spurred on improving the reversibility of the Mg

plating/stripping properties using the modification of organic electrolytes.

Grignard reagent with the general formula R-Mg-X/ethereal solutions (R = alkyl, aryl groups, and X = Cl, Br/or other halides) could obtain highly reversible Mg deposition-stripping and prevent the formation of passivation film [89]. In 2000, the first-generation electrolyte of RMBs was reported by Aurbach et al. [20] via using $Mg(AlCl_2BuEt)_2$ complex in tetrahydrofuran (THF) solution as an electrolyte, which exhibited reversible Mg deposition-dissolution characteristics and greatly promoted the development of rechargeable Mg batteries. However, the low anti-oxidation capability ($\approx$ 2.2 V $vs.$ Mg/Mg^{2+} RE (reference electrode)) of this electrolyte limits its use in RMBs with high energy density [90]. As a consequence, a high-voltage stable (> 3 V $vs.$ Mg/Mg^{2+} RE) all-phenyl complex (APC) electrolyte solution was designed [91]. It was theorized by replacing the organic ligand with the phenyl group, and the anodic stability window would increase by rendering the β-H elimination implausible (Fig. 9(a)) [92].

Chloride-containing electrolytes are still corrosive to all cell parts to some extent. The B-centered anions in the developed Mg electrolytes are completely compatible with Mg metal [79, 93]. The first B-based chloride-free electrolyte proposed by Mohtadi et $al.$ [94] was $Mg(BH_4)_2$ in THF/DME, which showed good electrochemical properties with stripping/plating onset potential at 0.03 V/–0.34 V and 67% cycling efficiency (40% in THF). The Coulombic efficiency and current density were significantly enhanced by the addition of $LiBH_4$ to $Mg(BH_4)_2$/DME electrolytes. A rechargeable Mg battery using Mo_6S_8 cathode and $LiBH_4/Mg(BH_4)_2$ in DME

electrolyte can remain 40 cycles at a current density of 128 mA g^{-1}. It is confirmed that introducing chelating ionic liquids can obtain a high degree of BH$_4^-$ dissociation from Mg(BH$_4$)$_2$ [64]. However, the low anodic stability and low Mg(BH$_4$)$_2$ solubility in a conventional ether solvent still limited their further development [95]. Recently, Cui's group [67] improved the electrochemical stability window to 2.8 V by using a multifunctional additive of tris(2H-hexafluoroisopropyl)borate (THFPB) to prepare the Mg(BH$_4$)$_2$/THFPB-diglyme electrolyte, which displayed an ionic conductivity of 3.72 mS cm^{-1} at 25 °C and Coulombic efficiency of 99%.

Mg(HMDS)$_2$-based (HMDS means Hexamethyldisilazide) electrolytes with high anodic stability, non-nucleophilic property, and high electrode compatibility have drawn great attention from researchers. However, the usual combination of Mg(HMDS)$_2$ with chloride salts limits their practical application due to the severe corrosion of cell components and low anodic stability. It was reported a chloride-free Mg(HMDS)$_2$-based electrolyte employing tetrabutylammonium borohydride (TBABH$_4$) as a moisture-scavenger additive instead of chloride-based additives [96]. The substitution of chloride-based additives for TBA$^+$ cation was due to its high reductive stability and possible electrostatic shielding effect on the Mg metal anode (Fig. 9(b, c)). Furthermore, the LiTFSI additive was introduced in Mg(HMDS)$_2$ electrolyte to effectively improve the discharge specific capacity of the sulfur cathode, causing a low discharge voltage of the Mg-S battery [97]. Interestingly, an effective method was proposed to reduce the polarization of the Mg electrode through *in situ* electrochemical activation under high current density, in which a Mg^{2+} ion conductive

film composed of inorganic/organic species can be formed, and the polarization of the Mg anode was significantly reduced. The electrochemical-driven interface conditioning can suppress the passivation of the Mg electrode in TFSI-containing electrolytes and enhance the electrochemical performance of the Mg-S battery.

Most of the above types of Mg electrolytes contain a large number of organometallic Mg complexes, and these electrolytes may be unfavorable to the safe use of RMBs. $Mg(TFSI)_2$-based electrolytes possess high solubility in various solvents, excellent ionic conductivity, and high oxidative stability (3.4 V vs. Mg/Mg^{2+} RE). However, due to the passivation reaction between impurities/TFSI$^-$ and Mg metal anode, electrolytes using single $Mg(TFSI)_2$ displayed large overpotential (> 2.0 V) and low Coulombic efficiency ($< 50\%$) during the Mg plating/stripping process. The introduction of additives into $Mg(TFSI)_2$ electrolytes was a necessary way to achieve reversible Mg deposition/dissolution and reduced overpotential. For example, it was reported the addition of BH_4^- effectively reduced the overpotential of the Mg anode and suppressed parasitic reactions [98]. To further improve the Mg plating and stripping metal anode, wang's group [79] introduced a family of methoxyethyl-amine chelates (hexadentate, tridentate, and bidentate) to 0.5 M $Mg(TFSI)_2$/DME electrolytes. Due to the solvation sheath reorganization, stable and highly reversible Mg metal batteries are achieved with energy densities of 412 W h Kg^{-1}.

Mg triflate ($Mg(OTf)_2$)-based electrolytes have shown significant promise for application in RMBs due to the high compatibility of OTf$^-$ with Mg anode and high Mg plating/stripping Coulombic efficiency. However, $Mg(OTf)_2$ shows low solubility

in ethereal solvents, which limits its practical application. To solve the problem, a high concentration of inorganic chloride ($MgCl_2$) was introduced to prepare an $Mg(OTf)_2$-based electrolyte by controlling the ratio between the two salts (i.e., $[Mg(OTf)_2]:[MgCl_2] > 1$), exhibiting excellent Mg stripping/plating Coulombic efficiency and uniform Mg deposition morphology [86]. Nevertheless, the ionic conductivity and rate capability of this electrolyte remain low. Subsequently, an organic chloride, tetrabutylammonium chloride (TBAC), was introduced as an effective electrolyte additive for $Mg(OTf)_2$-based electrolytes [86].

5.2. Solid-state electrolyte

Compared with organic electrolytes, Mg solid electrolytes have attracted more and more attention from researchers due to their good safety performances, high thermal stability, and excellent mechanical properties. The Mg solid-state electrolytes currently studied can be divided into the following three categories: organic solid-state electrolytes, inorganic solid-state electrolytes, and composite solid-state electrolytes, which will be summarized and discussed in this section.

Inorganic solid-state electrolytes refer to the general term of inorganic Mg^{2+} conductive materials, including oxides, chalcogenides, and hydrides, such as $Mg_{0.5}Zr_2(AsO_4)_6(PO_4)_3$, $Mg(BH_4)(BH_3NH_3)_2$, $MgS-P_2S_6-MgI_2$, which all have low ionic conductivity. Recently, researchers have attempted to optimize the preparation method, introduce a second phase, and develop other types of materials to enhance the conductivity of the inorganic solid-state electrolytes. For example, a new kind of chalcogenide spinels, i.e., MgX_2Z_4, with high Mg ion mobility was reported, where X

represents Y, Sc, and Z represents S, Se. The high-purity $MgSc_2Se_4$ phase exhibited a high ionic conductivity of 0.1×10^{-3} S cm^{-1} at room temperature as well as a low migration barrier of $\approx 370 \pm 90$ meV according to Mg nuclear magnetic resonance (NMR) relaxometry and electrochemical impedance spectroscopy (EIS) curves (Fig. 9(d–f)) [63]. The content of the Se element has an important effect on the electronic conductivity in a chalcogenide-rich phase, such as $MgSc_2Se_4$. Fichtner and co-workers [65] proposed the implementation of Se-rich phases, and Ti^{4+} and Ce^{4+} doping to lower the electronic conductivity but did succeed in obtaining an effective stratagem to reduce the electronic conductivity.

Organic solid-state electrolytes are formed by combining organic polymer and Mg salts such as $MgCl_2$, $Mg(ClO_4)_2$, $Mg(NO_3)_2$, $Mg(TFSI)_2$, and $Mg(OTf)_2$. Polyoxyethylene (PEO), polyvinylidene fluoride (PVDF) and polyvinylidene fluoride hexafluoropropylene (PVDF-HFP)), and polyvinyl alcohol (PVA) are the most investigated common organic polymer. Previous research has focused on simply mixing the organic polymer and Mg salts, such as $Mg(ClO_4)_2$-PEO and $MgCl_2$-PEO polymer electrolytes, which are incompatible with Mg metal electrodes, resulting in not meeting the need for high ionic conductivity. Researchers have attempted to mix polymer matrixes, plasticizers, and borate ester to enhance ionic conductivity. An Mg polymer electrolyte was prepared by using a novel porous PVDF-HFP membrane as polymer matrices and mixing $MgCl_2$-$AlCl_3$/TEGDME (Tetraethylene glycol dimethyl ether). The porous PVDF-HFP-based polymer electrolyte (PPE) possessed a high conductivity of 4.72×10^{-4} S cm^{-1} at 25 °C, as well as a wide voltage window of 3.1

V, and a low overpotentials of ~0.13 V in the Mg||Mg symmetric cell. They also achieved impressive long-cycle stability of 65.5 mA h g^{-1} over 1700 cycles in the MoS$_2$ cathode and Mg metal anode [99]. Moreover, MOFs have been widely investigated as novel ion-conductive materials with various ionic carriers. The pores of a MOF-based electrolyte, MIL-101⊃$_x$ (MIL-101 = Cr$_3$O(NO$_3$)(H$_2$O)$_2$(bdc)$_3$), where H$_2$bdc represented terephthalic acid, x = 0–1.7) were obtained by *in situ* mixture of MIL-101 with Mg(TFSI)$_2$. The MIL-101⊃$_{1.6}$ delivered a high Mg-ion conductivity of 1.9 × 10^{-3} S cm^{-1} at 25 °C, which exceeded all Mg^{2+}-containing crystalline compounds (Fig. 9(g, h)) [100].

Solid-state electrolytes are composed of a polymer electrolyte and an inorganic filler (e.g., TiO$_2$, MgO, Al$_2$O$_3$, SiO$_2$, CuS, ZrO$_2$), which can be regarded as composite polymer electrolytes (CPEs). Sun *et al*. [101] reported a composite solid electrolyte (Mg(TFSI)$_2$-PE) including PVDF-HFP, Mg(TFSI)$_2$, and SiO$_2$ nanoparticles in tetrahydrofuran/triethylene glycol dimethyl ether (THF/G3) solution. The Mg(TFSI)$_2$-PE displayed a highly reversible Mg^{2+} plating/striping capability and high ion conductivity (0.83 mS cm^{-1}). The full cell with a standardized cathode material of a layered titanic oxide cathode (H$_{0.68}$Ti$_{1.83}$O$_4$/rGO) using Mg(TFSI)$_2$-PE as the electrolyte exhibited a high energy density of ≈ 150 Wh kg^{-1} and an average voltage of 1.1 V [102].

5.3. Aqueous electrolyte

The aqueous RMBs are aqueous batteries composed of Mg metal as an anode and an aqueous solution as an electrolyte. It has advantages such as lower cost, higher

safety, higher ionic conductivity, and environmental friendliness. Therefore, aqueous RMBs are one of the most promising battery systems at present. However, the main reason why the Mg metal anode has not been able to be used as the anode of aqueous RMBs is that the free water activity of the electrolyte of the aqueous battery is too high, which leads to serious corrosion of Mg and produces a large amount of $Mg(OH)_2$. The rational design of electrolyte composition to inhibit the free water activity is the key to realizing Mg metal in aqueous Mg batteries [16, 103]. As a result, some researchers have proposed an aqueous Mg ion electrolyte solution of solvent-in-water and water-in-salt electrolyte by drawing on the design ideas of the electrolyte in aqueous zinc ion batteries and realized the uniform striping/plating of Mg metal in the aqueous electrolyte.

Recently, Chen's group [17] reported a strategy to control the accumulation of the passivation layer by designing a robust interfacial layer on an Mg metal anode using organic solvent-in-water (SIW) electrolytes. When the electrolyte consists of a series of x polyethylene glycol (PEG)/(1–x) H_2O ($0 < x < 50\%$) solvents with saturated $MgCl_2$ and 1 M $MnCl_2$ was conducted in aqueous Mg-MnO_2 batteries, the main compositions in the interfacial layer of the cycled Mg anode were MgO instead of conventional $Mg(OH)_2$ and $MgCO_3$ passivation layer, inhibiting free water from corroding the Mg metal anode. Due to building a strong H-bond (O···H-O) between PEG and H_2O, the water activity in the electrolyte was very low, and thus the Mg metal anode can be protected (Fig. 10(a–c)). They conducted the Mg‖Mg symmetric cells using SIW-2 (PEG:H_2O = 1:1) electrolytes and found that the polarization

voltage can be stabilized at around 30 mV over 750 min (Fig. 10(b)). In addition, the aqueous Mg-MnO$_2$ cell delivered a pronounced discharge plateau at $\approx$ 2.5 V and a high discharging capacity of $\approx$ 500 mA h g^{-1} over 1000 cycles (Fig. 10(d)). This result highlights the feasibility to protect the Mg metal anode by solvent-in-water-electrolyte engineering. Subsequently, a reversible aqueous Mg battery was achieved by converting their impermeable passivation films into conductive metal oxide complexes [17]. An MgCl$_2$ water-in-salt electrolyte (WIS) aqueous RMBs was proposed, which made Mg stripping/deposition reversible by converting the Mg passivation film into a conductive Mg-MgO interface (Fig. 10(e, f)). The MgCl$_2$ WIS electrolyte successfully preserved the Mg deposition and promoted Mg stripping by suppressing the hydrogen evolution reaction through the Cl-induced oxide layer (Fig. 10(g)). Using copper hexacyanoferrate (CuHCF) as the cathode, the obtained aqueous RMB exhibited an ultra-high discharge plateau of 2.4–2.0 V and operated over 700 cycles at 0.5 A g^{-1} with excellent stability. This work overcomes the passivation trend of Mg anodes, making it a viable and attractive option in RMBs.

6. Summary and perspective

RMBs are regarded as promising alternatives to LIBs owing to their high abundance, large volumetric energy density, and high safety. However, the development of Mg metal anode for RMBs is still in its infant stage and many limitations such as inhomogeneous Mg deposition/dissolution, surface passivation, and corrosion should be overcome before their commercial applications. In this review, we summarize some methods to deal with these problems.

Concerning uneven Mg deposition/dissolution and surface passivation in RMBs, four strategies are described above: 3D host nanostructure fabrication, Mg alloys anode design, surface modification, and electrolyte optimization. It is believed that all such approaches can suppress Mg nonuniform deposition/stripping as well as minimize the surface passivation of Mg metal anode, alleviate some of the drastic changes in volume, improve interfacial stability, and eventually enhance its electrochemical performance. Nevertheless, these modification strategies of Mg metal anode still face many challenges of the strong polarization effect, high-cost electrolytes, fast Mg metal anode degradation, and low compatibility between Mg metal anode and electrolytes in practical application.

Although notable progress has been made in this field of Mg metal anodes, it is anticipated to simultaneously develop a Mg metal anode with uniform Mg deposition/dissolution and low surface passivation via simple, low-cost, and environmentally friendly methods in the future. It is difficult to solve all the problems of Mg metal anodes via a single strategy; therefore, continuous multidisciplinary collaboration is highly profitable for the method innovation, paving the way for the practical applications of Mg metal anodes in RMBs. Several possible recommendations and perspectives need to be deeply considered.

(1) To understand the Mg deposition/stripping intensively. Mg deposition behavior is of great significance in guiding researchers to gain a profound understanding of stable Mg metal anode fabrication. In the case of the instability of Mg metal anode under characterization conditions, it is tough to analyze the evolution

of Mg anode during the Mg plating/stripping process. Some *in situ* characterization techniques from spectroscopic measurements and direct visualization such as *in situ* X-ray photoelectron spectroscopy (XPS), *in situ* X-ray absorption spectroscopy (XAS), *in situ* transmission electron microscopy (TEM), and *in situ* atomic force microscopy (AFM) should be employed to deeply investigate the dynamic nucleation, deposition and stripping processes on the electrode surface. Moreover, utilizing more theoretical calculations, such as density functional theory and phase field theory, would significantly improve the Mg deposition/dissolution mechanism to obtain high-performance RMBs.

(2) To establish a dendrite-free Mg alloy anode. Mg alloying is the most promising method for large-scale preparation. Generally, the electrochemical properties of alloys are dependent on the alloying elements, phase compositions, and microstructure. There are only very few studies that investigate the electrochemical behavior of Mg alloys anodes for RMBs. More Mg alloy systems with various compositions, microstructures, and manufacturing processes should be taken into consideration. By rational design of the composition, heat treatment, and manufacturing process, some special architectures, such as a homogeneous nano-sized precipitate or lamellar structure in the Mg matrix, can be achieved. The obtained novel microstructure is hopeful to fundamentally improve the Mg diffusion mode and accomplish a dendrite-free Mg alloy anode.

(3) To design a multifunctional artificial solid-electrolyte interphase. The artificial solid-electrolyte interphase strategy effectively protects the Mg metal by

reducing direct contact of the Mg with the electrolyte. Artificial solid-electrolyte interphase layers consisting of a single desired function cannot meet the standards of the complex working environment of Mg metal anode in different Mg-based battery systems (such as Mg-sulfur, Mg-iodine, and Mg-air). Composite or multilayered artificial solid-electrolyte interphase films with diverse features are in need of constructing stable interphase. An ideal artificial solid-electrolyte interphase layer should have the advantages of high Mg-ion conductivity, high flexibility, superior mechanical strength, and great environmental stability.

(4) To employ a safer electrolyte. Most common organic solvents with flammable properties can easily result in safety issues. Therefore, novel Mg-ion solid-state electrolytes and aqueous Mg ion electrolytes have attracted widespread attention. To date, the investigation of Mg solid-state electrolytes is still limited to obtaining novel materials with high Mg^{2+} conductivity at room temperature. Next, researchers should pay more attention to the electrochemical performance of Mg||Mg symmetric battery, as well as Mg-based full battery utilizing the novel Mg solid-state electrolytes. Reducing the interface impedance is still of significance to enhance the adhesion of the Mg metal anode and Mg solid-state electrolyte. In addition, an aqueous Mg electrolyte is a promising alternative choice. However, a few aqueous Mg electrolytes have not been employed in improving the Mg metal anode yet. More strategies, such as solvent-in-water and water-in-salt electrolytes, learning from the experience of designing electrolytes for aqueous Li/Na/K/Zn batteries, can be extensively investigated in future research.

(5) To develop suitable separators. Since separators hold close contact with all the components of RMBs, suitable separators are beneficial to improve battery performance. However, glass fiber most used type of separator in the field of RMBs is challenging to maintain the cyclability of anodes because they suffer from poor mechanical strength, fragile nature, and uneven ion transport channels. At present, few researchers have reported on the separator modification for RMBs. In terms of the Mg metal anode and separator being closely contacted in the battery configuration, two strategies can be employed for the separator in the future. Firstly, materials with high electrical conductivity or rich magnesiophilic functional groups can be used to modify the separator. Second, other membranes (such as Nafion membrane or other organic polymer membranes) with great magnesiophilicity can be used to take the place of the GF separator. Simultaneously, the mechanism study of separator modification is needed in future research.

Acknowledgments

References

[1] Y.Y. Liu, Y.Y. Zhu, Y. Cui, Nat. Energy 4 (2019) 540–550.

[2] Y.L. Liang, H. Dong, D. Aurbach, Y. Yao, Nat. Energy 5 (2020) 646–656.

[3] H.R. Bakhsheshi-Rad, M.H. Idris, M.R. Abdul-Kadir, A. Ourdjini, M. Medraj, M. Daroonparvar, E. Hamzah, Mater. Design 53 (2014) 283–292.

[4] Y.M. Zhao, A.B. Du, S.M. Dong, F. Jiang, Z.Y. Guo, X.S. Ge, X.L. Qu, X.H. Zhou, G.L. Cui, ACS Energy Lett. 6 (2021) 2594–2601.

[5] W.P. Zhao, Z.H. Pan, Y.J. Zhang, Y. Liu, H.L. Dou, Y.Y. Shi, Z.J. Zuo, B.W. Zhang, J.P. Chen, X.L. Zhao, X.W. Yang, Angew. Chem. Int. Edit. 61 (2022) e202205187.

[6] M. Rashad, M. Asif, I. Ahmed, Z. He, L. Yin, Z.X. Wei, Y. Wang, J. Magnes. Alloy. 8 (2020) 364–373.

[7] S.B. Son, T. Gao, S.P. Harvey, K.X. Steirer, A. Stokes, A. Norman, C. Wang, A. Cresce, K. Xu, C. Ban, Nat. Chem. 10 (2018) 532–539.

[8] F.F. Liu, T.T. Wang, X.B. Liu, L.Z. Fan, Adv. Energy Mater. 11 (2020) 2000787.

[9] R. Dominko, J. Bitenc, R. Berthelot, M. Gauthier, G. Pagot, V. Di Noto, J. Power Sources 478 (2020) 229027.

[10] P. Jankowski, R. Schwarz, A. Randon-Vitanova, R. Younesi, M. Wachtler, P. Johansson, Batteries Supercaps 4 (2021) 1335–1343.

[11] R.J.H. Thomas D. Gregory, Richard C. Winterton, J. Electrochem. Soc. 137 (1990) 775–780.

[12] C.L. Wei, L.W. Tan, Y.C. Zhang, B.J. Xi, S.L. Xiong, J.K. Feng, Y.T. Qian, Energy Storage Mater. 48 (2022) 447–457.

[13] Q. Luo, Y.L. Guo, B. Liu, Y.J. Feng, J.Y. Zhang, Q. Li, K. Chou, J. Mater. Sci. Technol. 44 (2020) 171–190.

[14] A. Hagopian, M. Doublet, J. Filhol, Energy Environ. Sci. 13 (2020) 5186–5197.

[15] C. Munteanu, B. Istrate, D. Mareci, S. Stanciu, C. Crimu, L.C. Trinca, E. Kamel, Environ. Eng. Manag. J. 15 (2016) 955–963.

[16] K.W. Leong, W.D. Pan, Y.F. Wang, S.J. Luo, X.L. Zhao, Dennis Y.C. Leung, ACS Energy Lett. 7 (2022) 2657–2666.

[17] Y. Xu, Z.C. Liu, X.H. Zheng, K, Li, M.M. Wang, W. Yu, H.L. Hu, W. Chen, Adv. Energy Mater. 12 (2022) 2103352.

[18] J. Cui, Z.W. Guo, J. Yi, X.Y. Liu, K. Wu, P.C. Liang, Q. Li, Y.Y. Liu, Y.G. Wang, Y.Y. Xia, J.J. Zhang, ChemSusChem 13 (2020) 2160–2185.

[19] C.S. Li, Y. Sun, F. Gebert, S.L. Chou, Adv. Energy Mater. 7 (2017) 1700869.

[20] D. Aurbach, Z. Lu, A. Schechter, Y. Gofer, H. Gizbar, R. Turgeman, Y. Cohen, M. Moshkovich, E. Levi, Nature 407 (2000) 724–726.

[21] R.Q. Zhang, Y. Lifshitz, S.T. Lee, Adv. Mater. 15 (2003) 635–640.

[22] Y.L. Liang, R.J. Feng, S.Q. Yang, H. Ma, J. Liang, J. Chen, Adv. Mater. 23 (2011) 640–643.

[23] D. Schloffer, S. Bozorgi, P. Sherstnev, C. Lenardt, B. Gollas, J. Power Sources 367 (2017) 138–144.

[24] R. Davidson, A. Verma, D. Santos, F. Hao, C. Fincher, S.S. Xiang, J. Van Buskirk, K. Xie, M. Pharr, P.P. Mukherjee, S. Banerjee, ACS Energy Lett. 4 (2019) 375–376.

[25] H.D. Lim, D.H. Kim, S. Park, M.E. Lee, H.J. Jin, S. Yu, S.H. Oh, Y.S. Yun, ACS Appl. Mater. Interfaces 11 (2019) 38754–38761.

[26] J. Eaves-Rathert, K. Moyer, M. Zohair, C.L. Pint, Joule 4 (2020) 1324–1336.

[27] J.H. Kwak, Y. Jeoun, S.H. Oh, S. Yu, J. Lim, Y. Sung, S. Yu, H. Lim, ACS Energy Lett. 7 (2022) 162–170.

[28] X. Liu, A.B. Du, Z.Y. Guo, C. Wang, X.H. Zhou, J.W. Zhao, F. Sun, S.M. Dong, G.L. Cui, Adv. Mater. 34 (2022) 2201886.

[29] Y. Li, G. Yang, S. Sun, C. Zhang, C.Y.J. Lim, A.J.Y. Wong, W.Y. Lieu, Z. Sofer, M.F. Ng, W. Liu, Z.W. Seh, Nano Lett. 22 (2022) 6808–6815.

[30] W. Jin, Z.G. Wang, Mater. Chem. Phys. 217 (2018) 388–392.

[31] J.Z. Niu, H. Gao, W.S. Ma, F.K. Luo, K.B. Yin, Z.Q. Peng, Z.H. Zhang, Energy Storage Mater. 14 (2018) 351–360.

[32] Y.Y. Hwang, N.K. Lee, S.H. Park, J. Shin, Y.J. Lee, Energy Storage Mater. 51 (2022) 108–121.

[33] D. Nguyen, A.Y.S. Eng, M. Ng, V. Kumar, Z. Sofer, A.D. Handoko, G.S. Subramanian, Z.W. Seh, Cell Rep. Phys. Sci. 1 (2020) 100265.

[34] B. Li, R. Masse, C.F. Liu, Y. Hu, W.S. Li, G.Q. Zhang, G.Z. Cao, Energy Storage Mater. 22 (2019) 96–104.

[35] H.D. Yoo, I. Shterenberg, Y. Gofer, G. Gershinsky, N. Pour, D. Aurbach, Energ. Environ. Sci. 6 (2013) 2265.

[36] J.Z. Niu, Z.H. Zhang, D. Aurbach, Adv. Energy Mater. 10 (2020) 2000697.

[37] Y. Zhang, M. Konya, A. Kutsuma, S. Lim, T. Mandai, H. Munakata, K. Kanamura, Small 15 (2019) 1902236.

[38] Y. Sun, F. Ai, Y.C. Lu, Small 18 (2022) 2200009.

[39] A. Maddegalla, A. Mukherjee, J.A. Blazquez, E. Azaceta, O. Leonet, A.R. Mainar,

A. Kovalevsky, D. Sharon, J.F. Martin, D. Sotta, Y. Ein Eli, D. Aurbach, M. Noked, ChemSusChem 14 (2021) 4690–4696.

[40] M. Jackle, A. Gross, J. Chem. Phys. 141 (2014) 174710.

[41] M.S. Ding, T. Diemant, R.J. Behm, S. Passerini, G.A. Giffin, J. Electrochem. Soc. 165 (2018) A1983–A1990.

[42] H.L. Dou, X.L. Zhao, Y.J. Zhang, W.Y. Zhao, Y.T. Yan, Z.F. Ma, X.M. Wang, X.W. Yang, Nano Energy 86 (2021) 106087.

[43] J. Muldoon, C.B. Bucur, A.G. Oliver, J. Zajicek, G.D. Allred, W.C. Boggess, Energy Environ. Sci. 6 (2013) 482–487.

[44] Z. Zhao-Karger, M.E. Gil Bardaji, O. Fuhr, M. Fichtner, J. Mater. Chem. A 5 (2017) 10815–10820.

[45] X.G. Li, T. Gao, F.D. Han, Z.H. Ma, X.L. Fan, S.Y. Hou, N. Eidson, W.S. Li, C.S. Wang, Adv. Energy Mater. 8 (2017) 1701728.

[46] D.J. Li, Y. Yuan, J.W. Liu, M. Fichtner, F.S. Pan, J. Magnes. Alloy. 8 (2020) 963–979.

[47] W.X. Wang, F.Y. Xiong, S.H. Zhu, J. Chen, J. Xie, Q.Y. An, eScience 2 (2022) 278–294.

[48] B.X. Wan, H.L. Dou, X.L. Zhao, J.H. Wang, W.Y. Zhao, M. Guo, Y.J. Zhang, J.J. Li, Z.F. Ma, X.W. Yang, ACS Appl. Mater. Interfaces 12 (2020) 28298–28305.

[49] Z.H. Song, Z.H. Zhang, A.B. Du, S.M. Dong, G.C. Li, G.L. Cui, Adv. Mater. 33 (2021) 2100224.

[50] X. Chen, X.R. Chen, T.Z. Hou, B.Q. Li, X.B. Cheng, R. Zhang, Q. Zhang, Sci.

Adv. 5 (2019) 1–9.

[51] J. Bae, H. Park, X.L. Guo, X. Zhang, J.H. Warner, G.H. Yu, Energy Environ. Sci. 14 (2021) 4391–4399.

[52] J. Liu, J.L. Zhang, Z.H. Zhang, A.B. Du, S.M. Dong, Z.F. Zhou, X.S. Guo, Q.F. Wang, Z.J. Li, G.C. Li, G.L. Cui, ACS Nano 16 (2022) 9894–9907.

[53] J.H. Kwak, S. Shin, Y. Jeoun, Y. Lee, S. Yu, Y.S. Yun, Y. Sung, S. Yu, H. Lim, J. Power Sources 541 (2022) 231724.

[54] C.L. Wei, L.W. Tan, Y.C. Zhang, Z.R. Wang, J.K. Feng, Y.T. Qian, Energy Storage Mater. 52 (2022) 299–319.

[55] T. Mandai, H. Somekawa, Chem. Commun. 56 (2020) 12122–12125.

[56] W.Z. Bao, R.H. Wang, B.Q. Li, C.F. Qian, Z.R. Zhang, J.F. Li, F.Y. Liu, J. Mater. Chem. A 9 (2021) 20957–20984.

[57] A.B. Ikhe, S.C. Han, S.J.R. Prabakar, W.B. Park, K. Sohn, M. Pyo, J. Mater. Chem. A 8 (2020) 14277–14286.

[58] X.C. Hu, S.Y. Lang, Y. Shi, R. Wen, L.J. Wan, J. Electroanal. Chem. 896 (2021) 115301.

[59] Q. Guo, W. Zeng, S.L. Liu, Y.Q. Li, J.Y. Xu, J.X. Wang, Y. Wang, Rare Metals 40 (2020) 290–308.

[60] R.N. Li, Q.S. Liu, R.P. Zhang, Y.Q. Li, Y.L. Ma, H. Huo, Y.Z. Gao, P.J. Zuo, J.J. Wang, G.P. Yin, Energy Storage Mater. 50 (2022) 380–386.

[61] X.Z. Chen, S.H. Wei, F.L. Tong, M.P. Taylor, P. Cao, Electrochim. Acta 398 (2021) 139336.

[62] F. Wang, D.Z. Wu, Y.C. Zhuang, J.L. Li, X.Z. Nie, J. Zeng, J.B. Zhao, ACS Appl. Mater. Interfaces 14 (2022) 31148–31159.

[63] P. Canepa, S.H. Bo, G. Sai Gautam, B. Key, W.D. Richards, T. Shi, Y. Tian, Y. Wang, J. Li, G. Ceder, Nat. Commun. 8 (2017) 1759.

[64] T. Watkins, A. Kumar, D.A. Buttry, J. Am. Chem. Soc. 138 (2016) 641–650.

[65] L.P. Wang, Z. Zhao-Karger, F. Klein, J. Chable, T. Braun, A.R. Schur, C.R. Wang, Y.G. Guo, M. Fichtner, ChemSusChem 12 (2019) 2286–2293.

[66] T.N. Chen, G.S. Gautam, P. Canepa, Chem. Mater. 31 (2019) 8087–8099.

[67] H.M. Xu, Z.H. Zhang, J.J. Li, L.X. Qiao, C.L. Lu, K. Tang, S.M. Dong, J. Ma, Y.J. Liu, X.H. Zhou, G.L. Cui, ACS Appl. Mater. Interfaces 10 (2018) 23757–23765.

[68] V. Bhaghavathi Parambath, Z. Zhao-Karger, T. Diemant, M. Jäckle, Z. Li, T. Scherer, A. Gross, R.J. Behm, M. Fichtner, J. Mater. Chem. A 8 (2020) 22998–23010.

[69] F. Tuerxun, K. Yamamoto, T. Mandai, Y. Tateyama, K. Nakanishi, T. Uchiyama, T. Watanabe, Y. Tamenori, K. Kanamura, Y. Uchimoto, J. Phys. Chem. C 124 (2020) 28510–28519.

[70] Y.J. Li, X.J. Zhou, J.L. Hu, Y.J. Zheng, M.S. Huang, K. Guo, C.L. Li, Energy Storage Mater. 46 (2022) 1–9.

[71] L.G. Kristensen, M.B. Amdisen, L.N. Skov, T.R. Jensen, Phys. Chem. Chem. Phys. 24 (2022) 18185–18197.

[72] X.S. Ge, F.C. Song, A.B. Du, Y.J. Zhang, B. Xie, L. Huang, J.W. Zhao, S.M. Dong, X.H. Zhou, G.L. Cui, Adv. Energy Mater. 12 (2022) 2201464.

[73] L.P. Wang, Z.Y. Li, Z. Meng, Y.L. Xiu, B. Dasari, Z.R. Zhao Karger, M. Fichtner,

Energy Storage Mater. 48 (2022) 155–163.

[74] H. Park, H. Lim, S.H. Oh, J. Park, H. Lim, K. Kang, ACS Energy Lett. 5 (2020) 3733–3740.

[75] J.L. Zhang, S. Wang, W.H. Wang, B.H. Li, J. Energy Chem. 66 (2022) 133–139.

[76] Z. Wang, A. Bandyopadhyay, H. Kumar, M. Li, A. Venkatakrishnan, V.B. Shenoy, E. Detsi, J. Energy Storage 23 (2019) 195–201.

[77] Y. Wang, E. Sahadeo, S.B. Lee, ACS Appl. Energy Mater. 5 (2022) 2613–2620.

[78] Y.J. Zhang, J. Li, W.Y. Zhao, H.L. Dou, X.L. Zhao, Y. Liu, B.W. Zhang, X.W. Yang, Adv. Mater. 34 (2022) 2108114.

[79] S.Y. Hou, X. Ji, K. Gaskell, P.F. Wang, L.N. Wang, J.J. Xu, R.M. Sun, O. Borodin, C. Wang, Science 374 (2021) 172–178.

[80] T. Yim, S.G. Woo, S.H. Lim, J.Y. Yoo, W. Cho, M.S. Park, Y.K. Han, Y.J. Kim, J. Yu, ACS Sustain. Chem. Eng. 5 (2017) 5733–5739.

[81] J.F. Song, J. Chen, X.M. Xiong, X.D. Peng, D.L. Chen, F.S. Pan, J. Magnes. Alloy. 10 (2022) 863–898.

[82] Q. Zhao, S. Stalin, L.A. Archer, Joule 5 (2021) 1119–1142.

[83] R.J. Lv, X.Z. Guan, J.H. Zhang, Y.Y. Xia, J.Y. Luo, Natl. Sci. Rev. 7 (2020) 333–341.

[84] C.L. You, X.W. Wu, X.H. Yuan, Y.H. Chen, L.L. Liu, Y.S. Zhu, L.J. Fu, Y.P. Wu, Y.G. Guo, T. van Ree, J. Mater. Chem. A 8 (2020) 25601–25625.

[85] R.P. Zhang, C. Cui, R.N. Li, Y.Q. Li, C.Y. Du, Y.Z. Gao, H. Huo, Y.L. Ma, P.J. Zuo, G.P. Yin, Chem. Eng. J. 426 (2021) 130751.

[86] D. Nguyen, A.Y.S. Eng, R. Horia, Z. Sofer, A.D. Handoko, M. Ng, Z.W. Seh, Energy Storage Mater. 45 (2022) 1120–1132.

[87] M.M. Huie, D.C. Bock, E.S. Takeuchi, A.C. Marschilok, K.J. Takeuchi, Coordin. Chem. Rev. 287 (2015) 15–27.

[88] L. Kong, C. Yan, J.Q. Huang, M.Q. Zhao, M. Titirici, R. Xiang, Q. Zhang, Energy Environ. Mater. 1 (2018) 100–112.

[89] Y.Q. Li, P.J. Zuo, R.N. Li, H. Huo, Y.L. Ma, C.Y. Du, Y.Z. Gao, G.P. Yin, R.S. Weatherup, ACS Appl. Mater. Interfaces 13 (2021) 24565–24574.

[90] N. Shrestha, K.S. Raja, V. Utgikar, J. Electrochem. Soc. 166 (2019) A3139–A3153.

[91] S. Chakrabarty, J.A. Blázquez, T. Sharabani, A. Maddegalla, O. Leonet, I. Urdampilleta, D. Sharon, M. Noked, A. Mukherjee, J. Electrochem. Soc. 168 (2021) 080526.

[92] B. Lee, J. Cho, H.R. Seo, S.B. Na, J.H. Kim, B.W. Cho, T. Yim, S.H. Oh, J. Mater. Chem. A 6 (2018) 3126–3133.

[93] H.D. Yoo, S.D. Han, I.L. Bolotin, G.M. Nolis, R.D. Bayliss, A.K. Burrell, J.T. Vaughey, J. Cabana, Langmuir 33 (2017) 9398–9406.

[94] R. Mohtadi, M. Matsui, T. Arthur, S. Hwang, Angew. Chem. Int. Ed. 124 (2012) 9918–9921.

[95] Y. Yan, J.B. Grinderslev, T. Burankova, S. Wei, J.P. Embs, J. Skibsted, T.R. Jensen, J. Phys. Chem. Lett. 13 (2022) 2211–2216.

[96] R. Horia, D.T. Nguyen, A.Y.S. Eng, Z.W. Seh, Nano Lett. 21 (2021) 8220–8228.

[97] Y.Q. Li, P.J. Zuo, R.N. Li, M.X. He, Y.L. Ma, Y.X. Shi, X.Q. Cheng, C.Y. Du, G.P. Yin, J. Energy Chem. 37 (2019) 215–219.

[98] Z. Ma, M. Kar, C.L. Xiao, M. Forsyth, D.R. MacFarlane, Electrochem. Commun. 78 (2017) 29–32.

[99] T.T. Wang, X.D. Zhao, F.F. Liu, L.Z. Fan, J. Energy Chem. 59 (2021) 608–614.

[100] Y. Yoshida, T. Yamada, Y. Jing, T. Toyao, K.I. Shimizu, M. Sadakiyo, J. Am. Chem. Soc. 144 (2022) 8669–8675.

[101] J.C. Sun, Y.B. Zou, S.Z. Gao, L.Y. Shao, C.C. Chen, ACS Appl. Mater. Interfaces 12 (2020) 54711–54719.

[102] A. Mallikarjun, M. Sangeetha, M.R. Mettu, M. Jaipal Reddy, J. Siva Kumar, T. Sreekanth, S. Venkateswara Rao, Mater. Today: Proc. 62 (2022) 5204–5208.

[103] Q. Li, L.S. Han, Q. Luo, X.Y. Liu, J. Yi, Batteries Supercaps 5 (2022) 1–25.

Table 1. A summary of the electrochemical performance of Mg alloys anodes in symmetric cells.

Materials	Liquid electrolyte	Cycling performance (h)	Current density (mA cm^{-2})	Capacity (mA h cm^{-2})	Overpotential (V)	Refs.
Mg-Ca		–	0.1	–	0.24	
		80	0.5	0.25	~0.67	
Mg-Ag		–	0.1	–	0.26	
		80	0.5	0.25	~0.80	
Mg-Bi		–	0.1	–	0.24	
		80	0.5	0.25	~1.06	
Mg-Zn	0.3 mol dm^{-3} Mg[B(HFIP)$_4$]$_2$/ Diglyme	–	0.1	-	0.25	[55]
		80	0.5	0.25	~1.06	
Mg-Y		–	0.1	–	0.18	
Mg-Mn		–	0.1	–	0.22	
Mg-Li		–	0.1	–	0.22	
Mg-Al		–	0.1	–	0.24	
Mg-Sn		–	0.1	–	0.24	
MgZn1.6		80	0.15	1.0	~0.67	
		24	1.0	1.0	~2.3	
MgGd1.6	(PhMgCl)$_2$-AlCl$_3$ /THF (APC)	80	0.15	1.0	~0.65	[23]
		24	1.0	1.0	~1.65	
MgZn1Gd1		80	0.15	1.0	~0.37	
		24	1.0	1.0	~1.8	
Mg1Sn	APC	150	0.05	0.03	0.14	[59]
Mg14Sn		150	0.05	0.03	0.19	
AZ31	APC	–	0.1	1.0	0.1	[39]
		–	1.0	1.0	0.5	

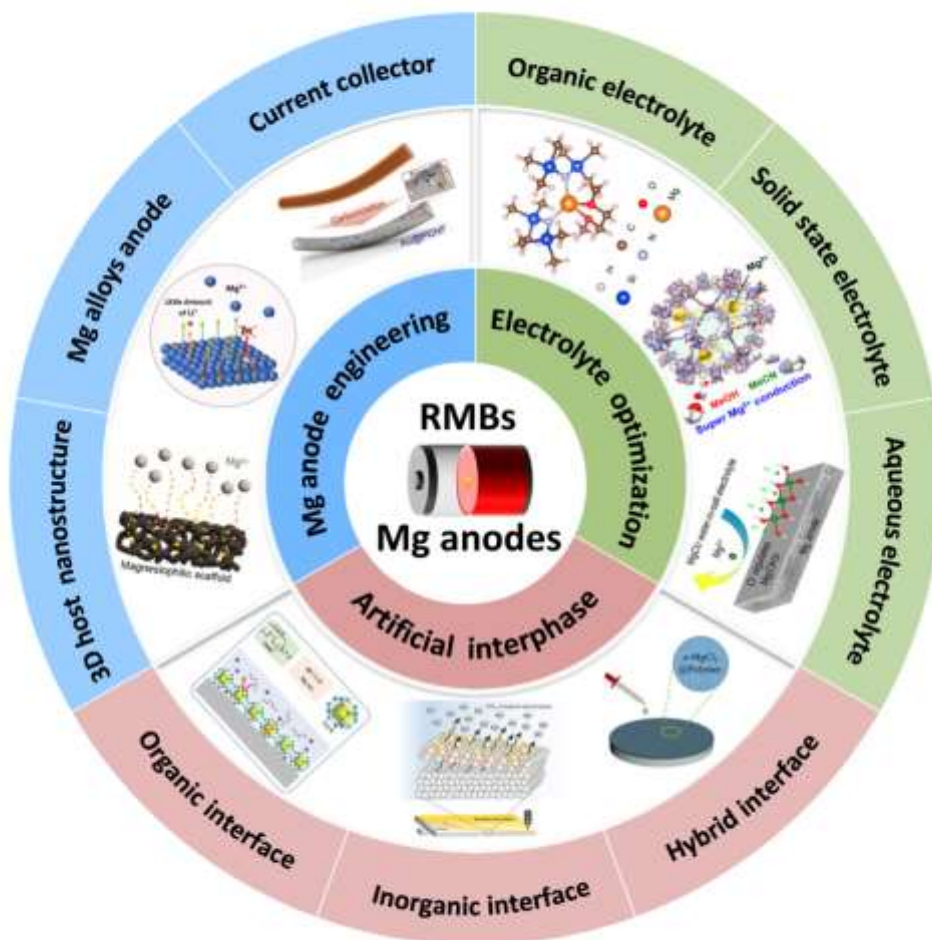**Fig. 1.** A timeline of the development of modification strategies for Mg metal anode.

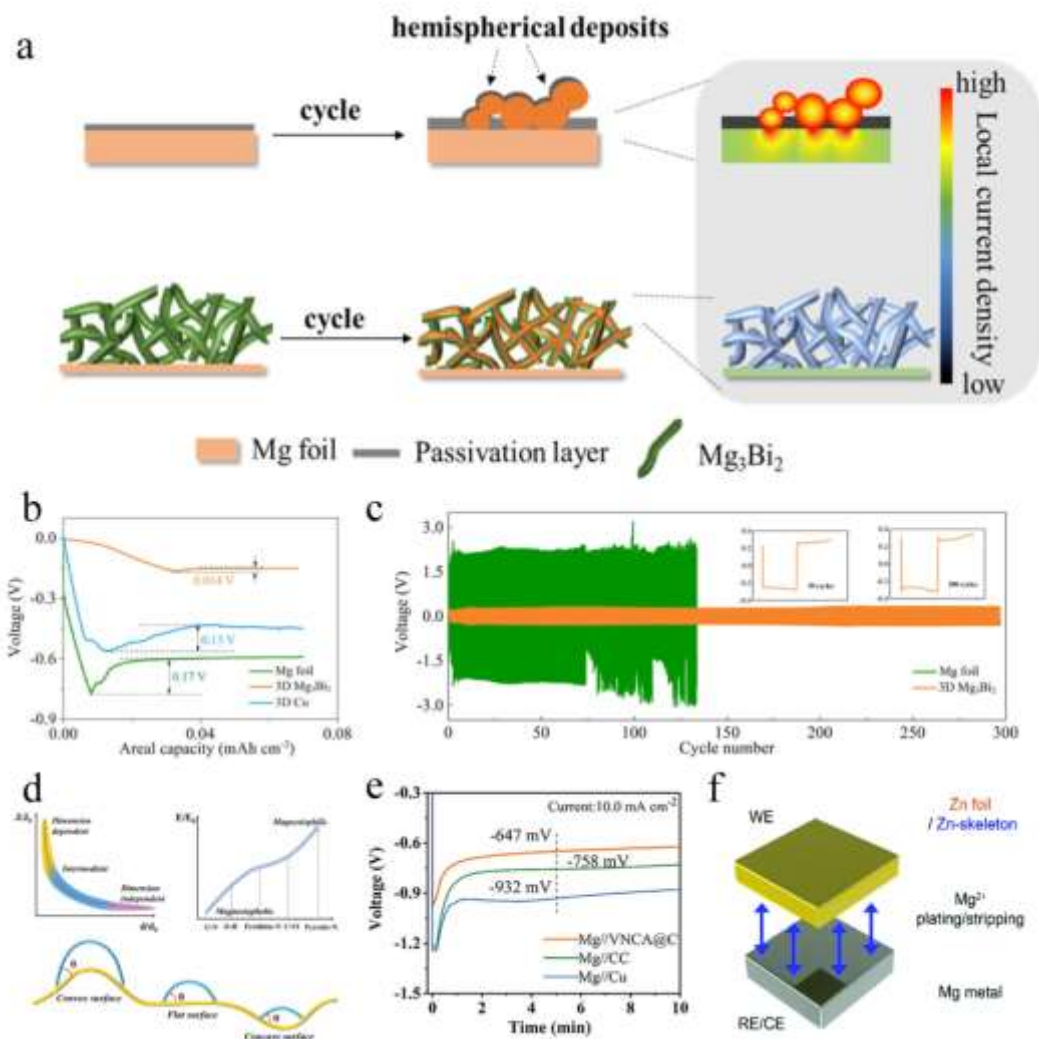**Fig. 2.** Schematic of modification strategies to improve the performance of Mg anodes for RMBs.

Fig. 3. (a) Scheme of the deposition morphology evolution on Mg foils and 3D Mg$_3$Bi$_2$. (b) Voltage profile of galvanostatic deposition on 3D Mg$_3$Bi$_2$, Mg foil, and 3D Cu at 0.01 mA cm^{-2}. (c) Galvanostatic cycling of symmetric cells with 30 min per cycle at 0.5 mA cm^{-2}. Reproduced with permission [48]. Copyright 2020, American Chemical Society. (d) Schematic illustration of design matrix for uniform Mg electrodeposition. (e) The overpotential of Mg//VNCA@C, Mg//CC, Mg//Cu at 10.0 mA cm^{-2}. Reproduced with permission [49]. Copyright 2021, Wiley-VCH. (f) Schematic illustration of Mg^{2+} plating/stripping on Zn foil or the Zn-skeleton in 0.5 M PhMgCl in THF electrolyte. Reproduced with permission [51]. Copyright 2021, The

Royal Society of Chemistry.
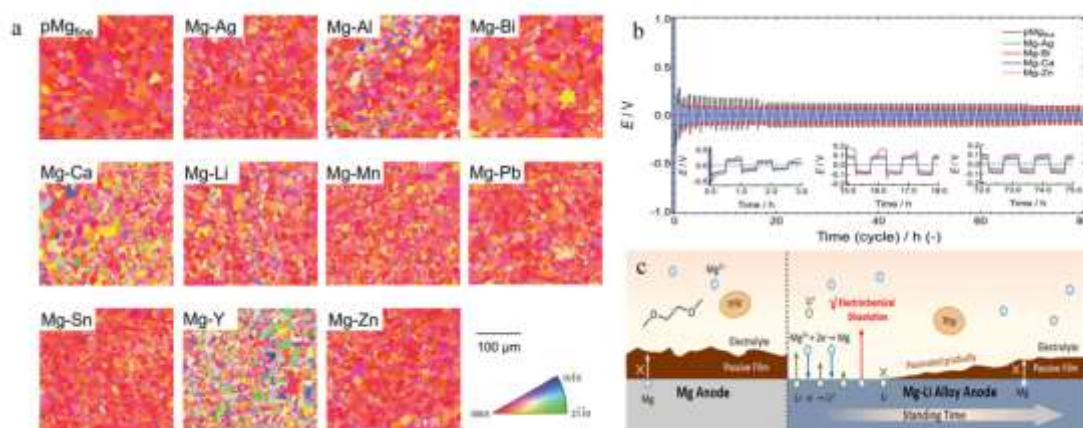
Fig. 4. (a) Electron Backscattered Diffraction (EBSD) maps of Mg–X. A color indicator for mirror indices is also shown. (b) Galvanostatic Mg dissolution/deposition (Mg^{2+}/Mg^0) cycling behaviour of pMg$_{fine}$ and the selected Mg–X cycled in 0.3 mol dm^{-3} Mg[B(HFIP)$_4$]$_2$/(diethylene glycol dimethyl ether, G2) at 30 °C. Reproduced with permission [55]. Copyright 2020, The Royal Society of Chemistry. (c) Schematic illustration of the passive film on Mg anode-electrolyte interface and the change of Mg-Li alloy anode/electrolyte interface withstanding time. Reproduced with permission [60]. Copyright 2022, Elsevier.
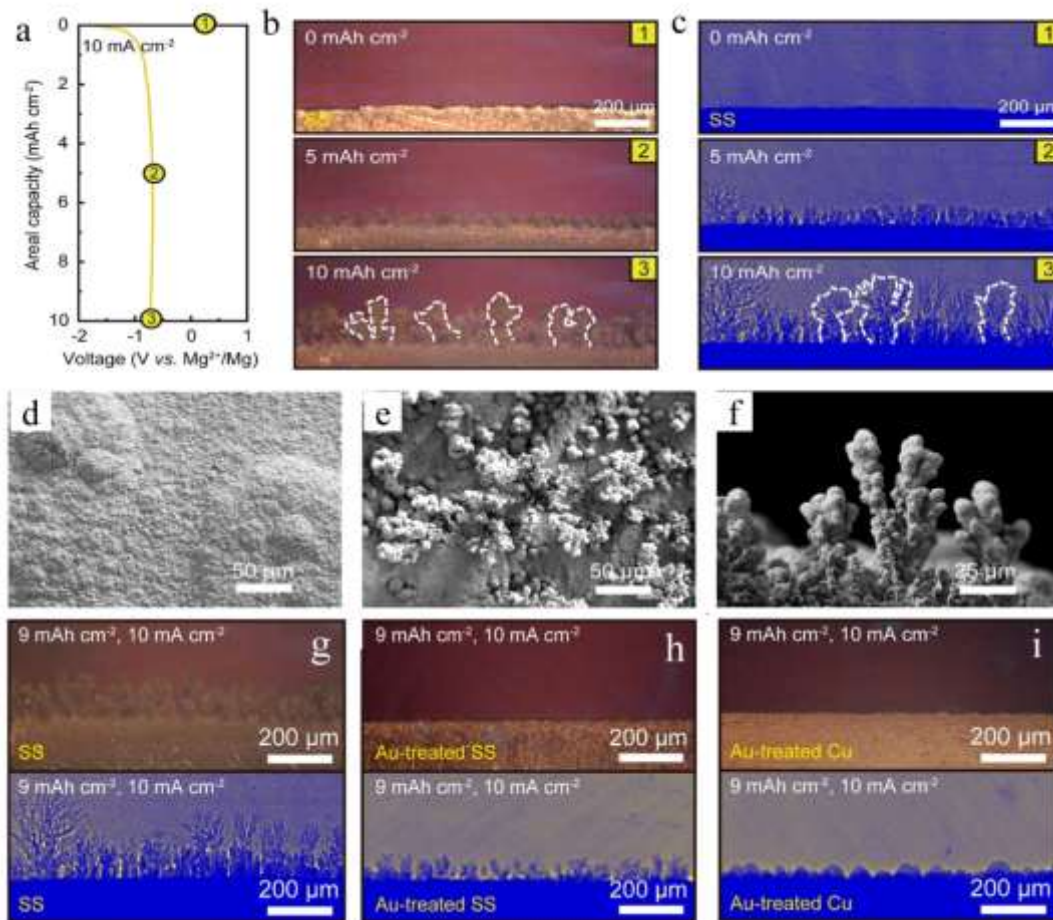
Fig. 5. (a) Electrochemical profile for Mg deposition at a current density of 10 mA cm^{-2} and corresponding cross-sectional images of Mg surface by (b) *operando* optical microscopy and (c) *operando* X-ray microscopy. Each image was captured at three stages of 0 (OCV), 5, and 10 mAh cm^{-2} as indicated by colored boxes. (d) *Ex situ* SEM images after the Mg depositions at (d) 2 mA cm^{-2} and (e, f) 10 mA cm^{-2}. Effect of Au magnesiophilic site for Mg deposition. (g–i) *Operando* optical and X-ray observations after Mg deposition to 9 mAh cm^{-2} at 10 mA cm^{-2}. Reproduced with permission [27]. Copyright 2022, American Chemical Society.
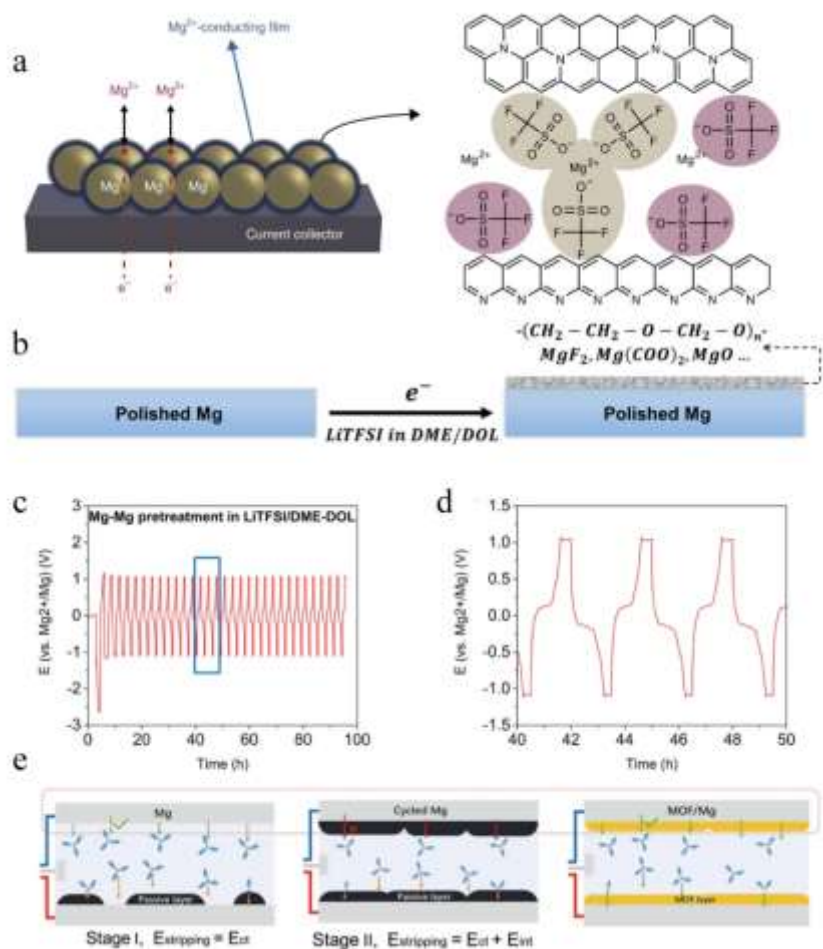
Fig. 6. (a) Schematic of an Mg powder electrode coated with the artificial Mg^{2+}-conducting interphase, and the proposed structure for the artificial Mg^{2+}-conducting interphase based on X-ray photoelectron spectroscopy (XPS), time of flight secondary ion mass spectrometry (TOF-SIMS) and thermal gravimetric analyzer (TGA). Reproduced with permission [7]. Copyright 2018, Springer Nature. (b) Scheme of electrochemical pretreatment of Mg metal anodes and the formation of the elastomeric ASEI, mainly consisting of poly-DOL. (c) Charging and discharging profile of the electrochemical pretreatment process at 0.03 mA cm^{-2} current density. (d) Zoomed-in region of the profile from 40 to 50 h. Reproduced with permission [77]. Copyright 2021, American Chemical Society. (e) Schematic illustration of the

stripping/plating process for bare Mg, cycled bare Mg, and MOF/Mg electrode, respectively. Reproduced with permission [78]. Copyright 2021, Wiley-VCH.
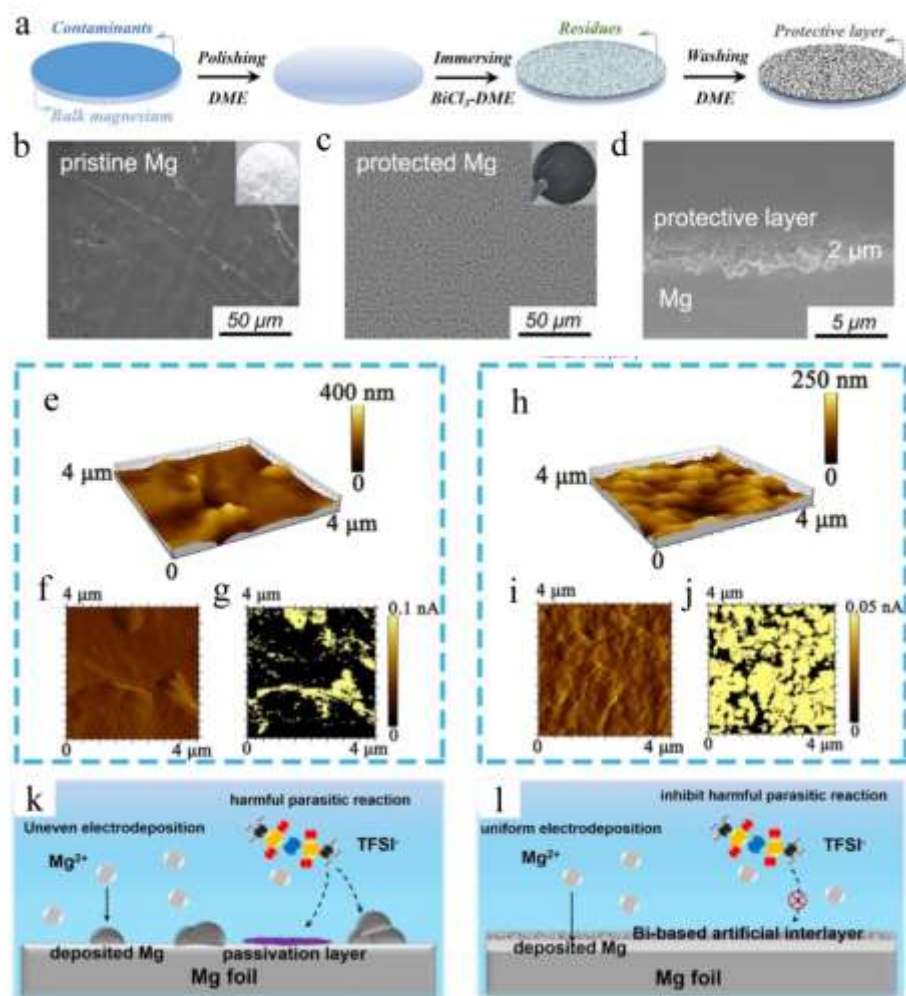
Fig. 7. (a) Schematic diagram of the preparation process of the protected Mg foil. (b) Surface SEM images of the pristine Mg foil. (c) Surface and (d) cross-sectional SEM images of the Bi-based protected Mg foil. (e–j) 3D, 2D morphology and corresponding surface conductivity mapping of atomic force microscopy (AFM) measurement on the pristine Mg surface (e–g) or the protected Mg surface (h–j) after electroplating Mg for 4 h at 1 mA cm^{-2}. (k, l) Schematic illustration of the electrochemical behavior at the interface between the Mg(TFSI)$_2$/DME electrolyte and the pristine Mg (k) or the protected Mg (l). Reproduced with permission [4]. Copyright 2021, American Chemical Society.
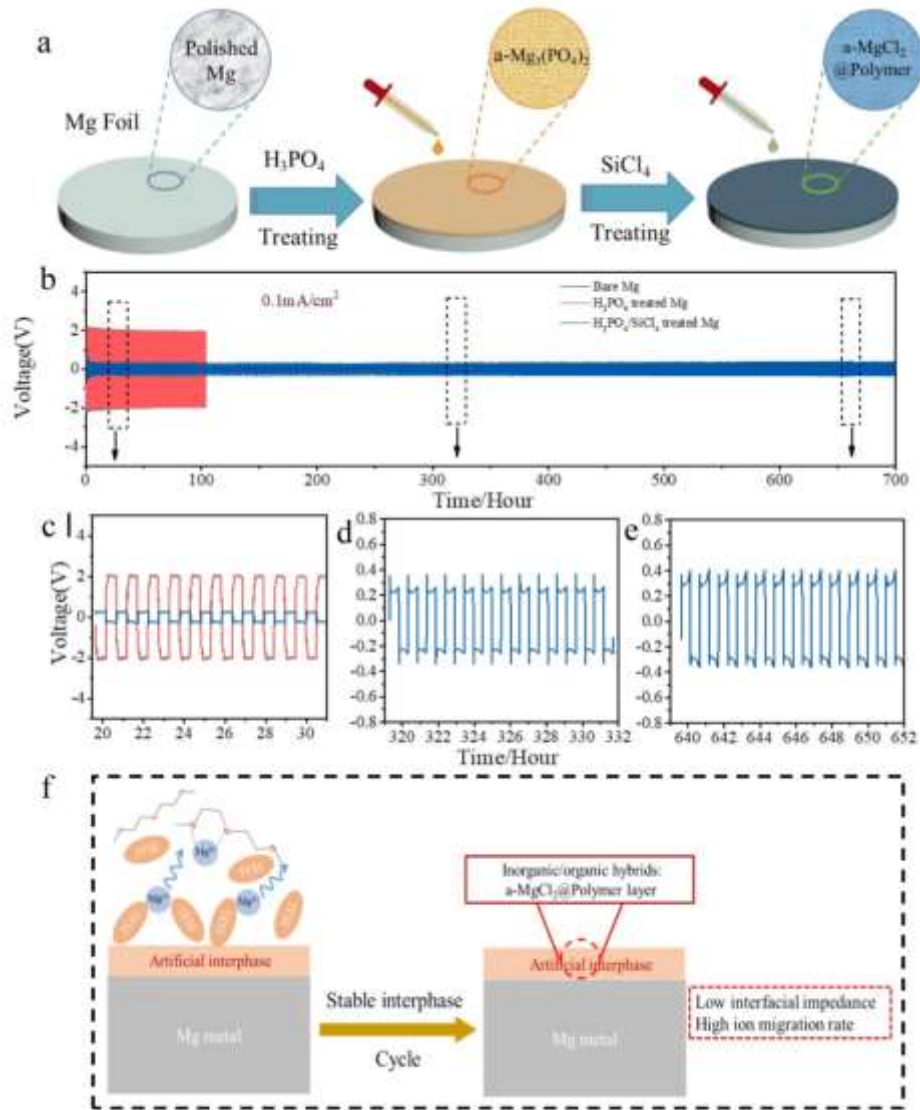
Fig. 8. (a) Illustration of the fabrication process for artificial interphase. (b) The cycling performance of the Mg-Mg symmetric cell with the bare Mg, H_3PO_4-treated Mg, and $H_3PO_4/SiCl_4$-treated Mg as the electrode in 0.5 M $Mg(TFSI)_2$/(Ethylene glycol dimethyl ether, G1) electrolytes at 0.1 mA/cm^{-2} for 1/2 h discharge and 1/2 h charge; (c–e) The voltage profile at a different time from to (b). (f) Schematic diagram of the action of artificial interphase. Reproduced with permission [85]. Copyright 2022, Elsevier.
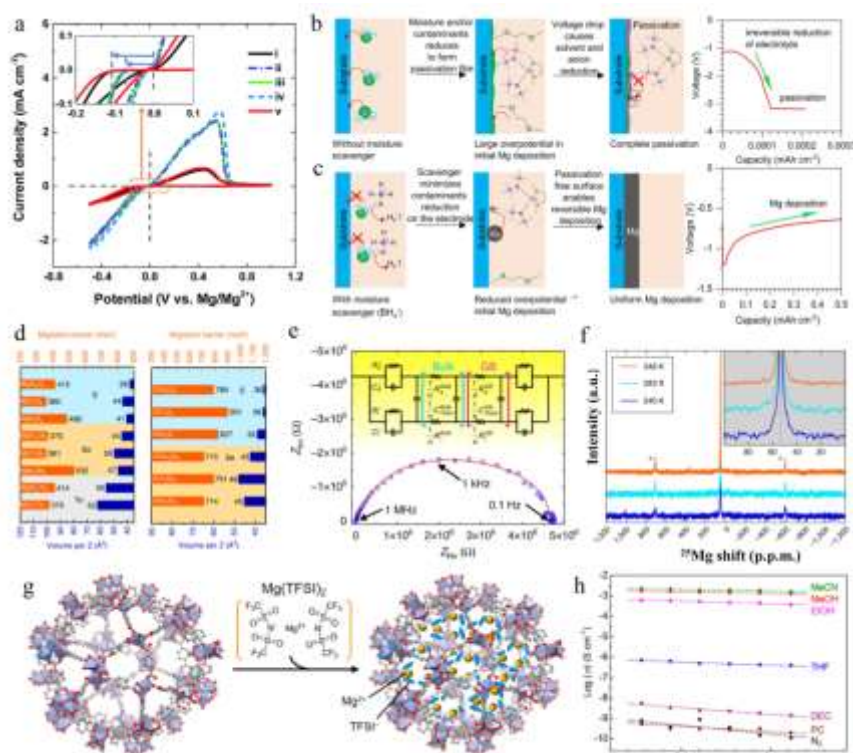
Fig. 9. (a) Cyclic voltammograms (5th cycle) and of Mg deposition-stripping for a series of electrolytes combining 0.4 M PhMgCl with a different molar concentration of AMPyrrCl in THF: (i) 0 M, (ii) 0.1 M, (iii) 0.2 M, (iv) 0.3 M, and (v) 0.4 M of AMPyrrCl. Reproduced with permission [92]. Copyright 2018, The Royal Society of Chemistry. (b, c) Schematic illustration of Mg deposition process (b) without and (e) with moisture scavenger in the electrolyte, respectively. Reproduced with permission [96]. Copyright 2021, American Chemical Society. (d) Computed Mg and Zn migration barriers (orange bars in meV) in AX_2Z_4 spinel and volume per anion (blue bars) using first-principles calculations. (e) Impedance spectrum of the Ta/MgSc$_2$Se$_4$/Ta cell, and the circuit utilized in the fitting of the impedance data. (f) Stack plot of 25 Mg magic angle spinning (MAS) variable temperature NMR of MgSc$_2$Se$_4$ collected at 11.7 T with a spinning speed of 20 kHz. Reproduced with permission [63]. Copyright 2017, Springer Nature. (g) Schematic illustration of

Mg(TFSI)$_2$ inclusion inside the pores of MIL-101. (h) Temperature dependence of ionic conductivity of MIL-101⊃$_{1.6}$ under various guest vapors or dry N$_2$. Reproduced with permission [100]. Copyright 2022, American Chemical Society.
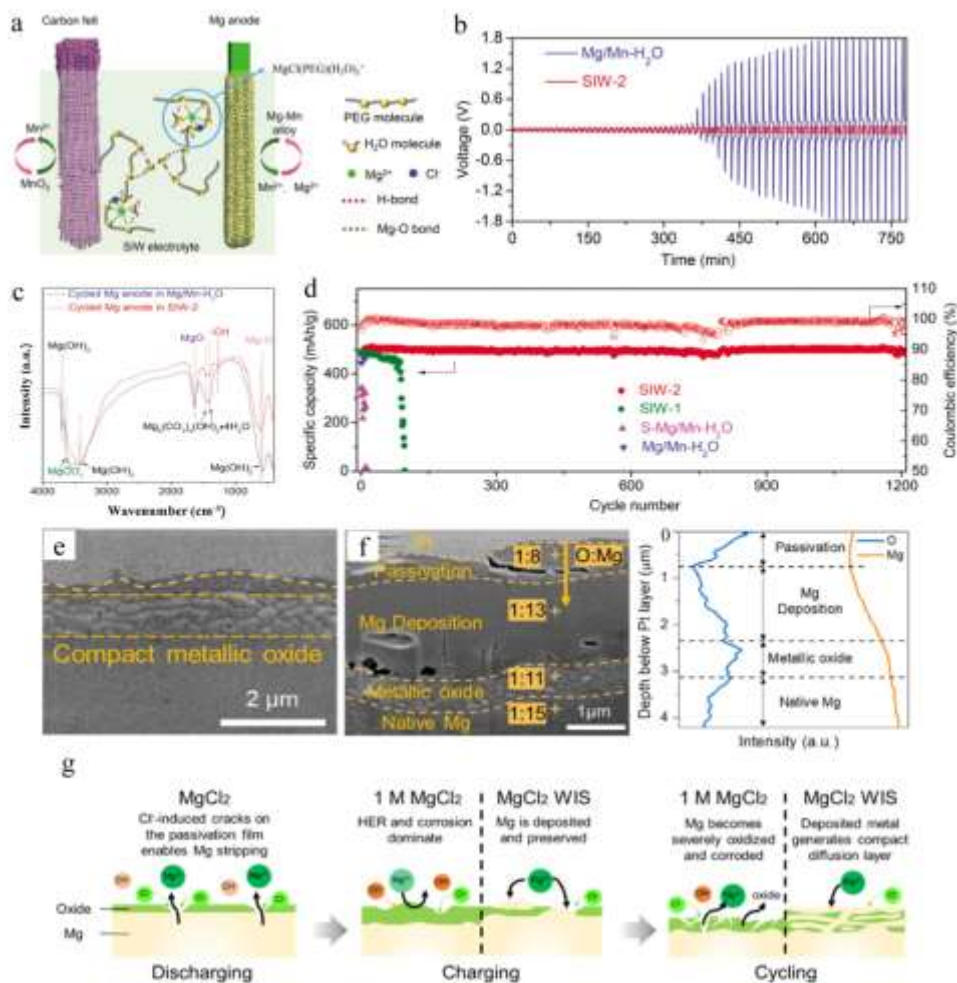
Fig. 10. (a) A schematic illustration of the Mg-MnO$_2$ battery in the charge and discharge modes. (b) Cycling stability of Mg||Mg symmetric cell in the electrolytes of Mg/Mn-H$_2$O and SIW-2 at the current density of 1 mA cm^{-2}. (c) Fourier transform infrared (FTIR) spectroscopy of cycled Mg anode in the electrolytes of Mg/Mn-H$_2$O and SIW-2. (d) Cycling stability of Mg-MnO$_2$ cells in different electrolytes at 5 C. Reproduced with permission [17]. Copyright 2021, Wiley-VCH. (e) Cross-sectional FIB-SEM images of the Mg anode after five cycles in an Mg||Mg symmetrical cell under MgCl$_2$ WIS. (f) Cross-sectional FIB-SEM image (left panel) and EDS line scans (right panel) of the Mg anode after 200 cycles in an Mg||Mg symmetrical cell in MgCl$_2$ WIS. The orange arrow shows the line scan location. (g) Schematic illustration

of the Mg stripping/plating mechanism in aqueous $MgCl_2$. Reproduced with permission [16]. Copyright 2022, American Chemical Society.